# Control of successive unequal cell divisions by neural cell fate regulators determines embryonic neuroblast cell size

T. W. Mullan[1], T. Felton[1], J. Tam[1], O. Kasem[1], T. J. Yeung[1,‡], N. Memar[1,2,§], R. Schnabel[2], and R. J. Poole[1,*]

[1]Department of Cell and Developmental Biology, University College London, London WC1E 6BT, UK
[2]Institut für Genetik, TU Braunschweig, Braunschweig, Germany

[*]Corresponding author: r.poole@ucl.ac.uk
[‡]Present address: The Francis Crick Institute, London, NW1 1AT
[§]Present address: Center for Genomic Integrity, Institute for Basic Science (IBS), Ulsan 44919, South Korea

**Keywords**: asymmetric division, neuronal specification, proneural, *C. elegans*

## Abstract

Asymmetric cell divisions often generate daughter cells of unequal size in addition to different fates. In some contexts, daughter cell size asymmetry is thought to be a key input to specific binary cell fate decisions. An alternative possibility is that unequal division is a mechanism by which a variety of cells of different sizes are generated during embryonic development. We show here that two unequal cell divisions precede neuroblast formation in the C lineage of *C. elegans*. The equalisation of these divisions in a *pig-1/MELK* mutant background has little effect on neuroblast specification. Instead, we reveal *let-19/MDT13* as a novel regulator of the proneural bHLH transcription factor *hlh-14/ASCL1* and find that both are required to concomitantly regulate the acquisition of neuroblast identity and neuroblast cell size. Thus, embryonic neuroblast cell size in this lineage is progressively regulated in parallel with identity by key neural cell fate regulators. We propose that key cell fate determinants have a novel function to regulate unequal cleavage and therefore cell size of the progenitor cells whose daughter cell fates they then go on to specify.

## Introduction

The development of multicellular organisms generates various cell types, each with its own unique molecular signature and specific cell size. Asymmetric cell division

is one mechanism by which two daughter cells can acquire different fates (reviewed in Horvitz and Herskowitz, 1992). That asymmetric cell divisions can also generate daughters of unequal sizes has been known for over 100 years, since embryonic studies of leech (Whitman, 1878), Ascaris nematode (Boveri, 1899) and Ascidian (Conklin, 1905) demonstrated asymmetric inheritance of developmental potentials and the establishment of cell lineages. However, why dividing cells regulate daughter cell size and whether this influences asymmetric fate specification remains unresolved.

The specification of asymmetric daughter cell fates during cell division is often established through asymmetric inheritance of fate determinants such as proteins, RNA or cellular organelles (reviewed in Gönczy, 2008; Horvitz and Herskowitz, 1992; Knoblich, 2008; Sunchu and Cabernard, 2020). Studies focused on the *C. elegans* zygote and *Drosophila* neuroblasts have revealed that asymmetric segregation of key fate determinants depends on cortical polarity established by the conserved PAR network. Cortical polarity then influences asymmetric segregation of key cell fate determining proteins such as PIE-1, MEX-5 and MEX-6 in the *C. elegans* zygote and Prospero, Numb and Brat in *Drosophila* neuroblasts (reviewed in Gönczy, 2008; Loyer and Januschke, 2020; Neumüller and Knoblich, 2009; Rose and Gönczy, 2014; Sunchu and Cabernard, 2020). Importantly, the asymmetric segregation of Prospero into daughter cells controls fate but does not control cell size (Doe et al., 1991).

The molecular mechanisms regulating unequal cleavage fall into two categories (reviewed in Sunchu and Cabernard 2020). One category is spindle-dependent and employs asymmetric spindle positioning or pulling forces via a conserved G-protein- and *lin-5/NuMa*-containing complex (Bowman et al., 2006; Nguyen-Ngoc et al., 2007; Siller et al., 2006; Srinivasan et al., 2003, Grill et al., 2001, Bonaccorsi et al., 2000; Fuse et al., 2003). The second is spindle-independent and includes asymmetric cortical myosin flows and hydrostatic pressures generating apical expansion (Cabernard et al., 2010; Pham et al., 2019; Roubinet et al., 2017; Tsankova et al., 2017). In *C. elegans* both spindle-dependent and spindle-independent mechanisms are evident in the post-embryonic Q lineage. Anterior enrichment of cortical myosin is required for the unequal cleavage of the posterior daughter of the Q cell, Q.p, whereas the anterior daughter Q.a depends on spindle-displacement (Ou et al., 2010). Both however depend on the kinase *pig-1/MELK*, a PAR-1 like kinase (Cordes et al., 2006; Feng et al., 2013). *pig-1/MELK* also regulates a number of other unequal cell divisions in the *C. elegans* embryo (Liro et al., 2017; Pacquelet et al., 2015; Cordes et al., 2006; Wei et al., 2017), many of which produce a daughter that undergoes apoptosis and a sister cell that is either a neuroblast or neuron

(Cordes et al., 2006; Wei et al., 2017). In the NSM neuroblast *pig-1/MELK* acts upstream of myosin and may directly phosphorylate it (Wei et al., 2020). In *pig-1/MELK* mutants loss of unequal division causes inappropriate survival of the cells normally fated to die, suggesting that cell size itself may affect the acquisition of apoptotic fate (Cordes et al., 2006). Inactivation of myosin in Q.a also leads to symmetric daughter cell size and daughter cell fate (Ou et al., 2010). In *Drosophila* neuroblasts, and the one-cell *C. elegans* zygote, manipulation of spindle asymmetry or asymmetric pulling forces symmetrises daughter cell size as well as disrupting daughter cell fates (Cabernard and Doe, 2009; Fuse et al., 2003; Jankele et al., 2021). However, it is unclear to what extent these manipulations affect cortical polarity and/or asymmetric segregation.

Many organisms, including nematodes and flies, have an indirect programme of development in which no cell growth occurs in the embryo and the majority of cell and organismal growth is confined to the post-embryonic larval stages (reviewed in O'Farrell, 2004). Yet, at the end of embryogenesis, the larvae produced hatch with fully developed tissues containing cells of a variety of different sizes appropriate to their function. This raises an alternative hypothesis that the regulation of unequal cleavage may be used to generate cells of different sizes during development, particularly in situations where no cell growth is possible. Here we show that DVC neuroblast formation in the *C. elegans* C lineage, the specification of which requires the expression of proneural bHLH transcription factor *hlh-14/ASCL1* (Poole et al., 2011), is preceded by two distinctly unequal cleavages. We find that *pig-1/MELK* regulates these unequal cleavages, yet symmetrisation of daughter cell size in this mutant background has little effect on the expression of *hlh-14/ASCL1* in the DVC neuroblast, its specification, nor the production of the DVC neuron. We reveal that the mediator complex component *let-19/MDT13* is a novel regulator of the proneural bHLH transcription factor *hlh-14/ASCL1* and find that both factors concomitantly regulate the acquisition of neuroblast identity and neuroblast cell size, the latter via the regulation of unequal cleavage. Thus, cell size does not direct proneural gene expression but instead is regulated in parallel with terminal identity to coordinate the cellular and molecular aspects of DVC specification. We propose that the regulation of unequal cleavage by key cell fate determinants is a mechanism to generate cell size differences in the absence of cell growth.

## Results

### Two unequal cleavages precede *hlh-14 e*xpression in the DVC neuroblast

The C lineage comprises two nearly bilaterally symmetric halves derived from the daughter cells Ca and Cp. Defining left-right asymmetry in the lineage, the anterior half of lineage descended from Ca contains the neurons DVC and PVR, whose bilateral homologues descended from Cp are hypodermal(epidermal) (Fig. 1A) (Sulston et al., 1983). Like many divisions in the *C. elegans* embryo, those preceding the production of DVC and PVR are asymmetric in fate. The division of Caa represents a decision between an anterior non-neural ectodermal branch and a posterior neural/non-neural ectodermal branch (Fig. 1A). The subsequent division of Caap represents a decision between an anterior neural/cell death branch and a posterior neural and non-neural ectodermal branch; the DVC neuroblast and the PVR/HYP7 neural/non-neural ectodermal cells respectively (Fig. 1A).

Through 4D-lineage analysis and volumetric quantifications we find that these two asymmetric cell divisions are also unequal in size. Caaa is over twice the size of Caap, and Caapp is twice that of Caapa (Fig. 1B, C). In contrast we find most other divisions in the C lineage exhibit either an equal cleavage or an unequal cleavage with a very small bias towards to the anterior cell (Fig. 1B,C), consistent with previous reports (Arata et al., 2014; Fickentscher and Weiss 2017). The two most overtly unequal cleavages in the C lineage, those of Caa and Caap, differ significantly in their volume ratio to the bilaterally homologous divisions, which do not generate neurons (Fig. 1A,C). In addition to the conservation of C lineage topology in many Rhabditida species (Houthoofd et al., 2003; Houthoofd et al., 2008; Memar et al., 2019; Zhao et al., 2008) we find that the unequal cleavages of Caa and Caap are also mmaxaconserved over at least 20M years of evolution in the *Caenorhabditis* genus (Fig. S1). Our lineage analysis also indicates the conservation of the programmed cell death of Caapap and, based on cell position and nuclear morphology, it is highly likely that Caapaa is also a neuron in these species (Fig. S1). Given such conservation we investigated whether unequal cell size may be required for neural fate decisions in the lineage and ultimately DVC neuroblast specification.

### C lineage unequal cleavages are equalised in *pig-1(gm344)* and *ham-1(n1438)* mutants

We have previously shown that the specification of DVC depends on the proneural bHLH transcription factor *hlh-14/ASCL1* in the DVC neuroblast Caapa ((Poole et al., 2011); Fig. 1A). In *hlh-14* null mutants, as well as conversion to hypodermal fate, the

would-be DVC neuroblast divides precociously at the same time as the C lineage hypoblasts (Poole et al., 2011). To assess whether the unequal cleavages and resultant unequal daughter sizes are required for the expression of *hlh-14* in Caapa, we sought to equalise these cleavages. The MELK kinase PIG-1 is involved in many unequal neuroblast divisions (Cordes et al., 2006; Feng et al., 2013; Wei et al., 2020). Not previously implicated in the C lineage, we confirmed expression of *pig-1* in both Caa and Caap using a transcriptional reporter (Fig. 2A). We also find that in *pig-1(gm344)* mutants, a strong loss of function allele, the cleavages of both Caa and Caap are equalised (Fig. 2B,C; Fig S2). We also observed that the DVC neuroblast Caapa divides precociously in a large proportion of lineaged embryos (Fig. 2D and Fig. S3A). To control for different developmental rates between genotypes we also assessed this precocious division as a ratio between the cell cycle duration of Caapa and its sister Caapp. This analysis comprised additional lineaged embryos to those measured for cell volume ratio (Fig. 2D and Fig. S3B).

The STOX transcription factor HAM-1 is broadly expressed in the embryo and is also a known regulator of many unequal neuroblast divisions, particularly those that generate a smaller anterior cell (Frank et al., 2005; Guenther and Garriga, 1996; Leung et al., 2016; Teuliere et al., 2018). In the Q lineage it is a thought to act as a regulator of *pig-1* (Feng et al., 2013). In contrast to *pig-1(gm344)* mutants, in embryos carrying the loss of function *ham-1(n1438)* allele the volume ratio of the Caa cleavage retains an anterior bias (Fig. 2B,C). The Caap cleavage however, demonstrates a significant reduction in volume ratio and a tendency towards equalisation (Fig. 2B,C; Fig. S2). As with *pig-1(gm344)*, a significant proportion of *ham-1(n1438)* embryos display a precocious Caapa division. This analysis included an additional embryo to those measured for cell volume ratio (Fig. 2D and Fig. S3). Taken together, these results indicate the novel findings that *pig-1* controls unequal cleavage of both the Caa and Caap blastomeres and *ham-1* that of Caap. *pig-1* and *ham-1* mutants are therefore good genetic backgrounds in which to assess the role of these unequal cleavages on the acquisition of asymmetric daughter cell fates, particularly the asymmetric expression of *hlh-14* in Caapa.

**Equalisation of the Caa or Caap blastomere cleavages in *pig-1* and *ham-1* mutants has little effect on *hlh-14* expression in the DVC neuroblast Caapa**

4D-lineage analysis using a translational fusion reporter revealed that the equalisation of the Caap blastomere cleavage in *ham-1(n1438)* embryos has no effect on the expression of *hlh-14. hlh-14* was detected in Caapa and, after division, in its daughters

Caapaa (DVC) and Caapap (death) in 10/10 lineaged embryos, which includes those nine measured in Fig. 2 (Fig. 3A,B). Similarly, despite equalisation of both cleavages in *pig-1(gm344)* embryos, *hlh-14* was expressed in the DVC neuroblast Caapa in 23/26 lineaged embryos in which expression could be analysed, including all those measured for Caa and Caap in Fig. 2. 24/26 continued to express *hlh-14* in Caapaa and Caapap following division (Fig. 3A,B). Furthermore, transgene expression was never evident in an ectopic branch. For example, equalisation of the Caa cleavage did not result in ectopic expression in Caaa or any of its descendants (Fig. S5 and Fig. S6).

Assessment of *hlh-14* expression was also conducted using another, fosmid-based translational fusion reporter. As in *wild type* embryos, both *pig-1(gm344)* and another strong loss of function allele *pig-1(tm1510)* displayed *hlh-14* expression in the DVC neuroblast and its descendants in all lineaged embryos (Fig. 3B,C). In addition to expressing *hlh-14*, the position of the DVC neuroblast Caapa in *pig-1* and *ham-1* resembles that observed in *wild type* embryos, occupying a central position in the posterior of the embryo during the C16 stage (Fig. 4A). This contrasts *hlh-14* mutants in which Caapa migrates to a lateral position at the same stage, adjacent to hypodermal cells, itself having adopted hypodermal fate (Poole et al., 2011). Unlike the translational reporter, the fosmid-based reporter is also expressed in the PVR neuron. We found that *hlh-14* was expressed in Caappa (PVR) in all lineaged *pig-1* mutant embryos (Fig. 3B,C). Taken together these results suggest that the unequal cleavages of the Caa and Caap blastomeres and resultant smaller daughter cell sizes are not the main factor determining asymmetric expression of *hlh-14* in the DVC neuroblast (Caaapa) and the PVR neuron.

### ***pig-1*** **and** ***ham-1*** **affect the asymmetric division of the DVC neuroblast**

We next asked whether cleavage equalisation affects later steps in C lineage neurogenesis downstream of *hlh-14* expression. Specifically, we examined if the Caapaa blastomere still acquires DVC fate. This was assessed in the same embryos using a transcriptional fusion reporter for the DVC specific transcription factor *ceh-63* (Feng et al., 2012). Although *hlh-14* and *ceh-63* expression were both assessed with GFP transgenes in the same animal, they could be assessed simultaneously in the same 4D-lineaged embryo since they are expressed at different embryonic stages in a non-overlapping manner and because the *hlh-14::gfp [gmIs20]* reporter is nuclear whilst the *ceh-63::gfp* reporter is cytoplasmic. A further two *pig-1(gm344)* mutant embryos in addition to the 26 lineaged for *hlh-14* expression (Fig. 3) were assessed for *ceh-63* expression. The majority display a single DVC neuron; 6/28 embryos lack a neuron and 4/28 displayed two

neurons. (Fig 4A,B). In hatched L1 *pig-1(gm344)* larvae both single and ectopic DVC neurons display a normal morphology and display neuronal processes (Fig. S4). As with the equalisation phenotypes, these phenotypes are weaker in *ham-1(n1438)* mutants where all embryos display a single neuron (Fig. 4A,B).

Lineage analysis revealed that *pig-1(gm344)* mutants display a range of terminal DVC neuroblast division defects akin to those described in other lineages (Cordes et al., 2006; Ou et al., 2010; Feng et al., 2013; Zhu et al., 2014; Wei et al., 2017). Only 3/28 lineaged embryos displayed a *wild type* fate pattern at the terminal division (Fig. S5). The remaining 25/28 embryos displayed an asymmetry defect at the terminal division, with the inappropriate survival of Caapap, and subsequent adoption of DVC fate by one, both or neither of Caapaa and Caapap (Fig. 4C and Fig S5). 18/25 of these embryos displayed a precocious division of Caapa (the DVC neuroblast). In 6/18 of those embryos Caapa daughter cells underwent an extra round of division (Fig. 4C and Fig. S5). This resulted in supernumerary *hlh-14* expressing cells and so in some cases extra DVC neurons (Fig. S5). Extra divisions were confined to the Caapa branch with the supernumerary DVCs arising from either the inappropriately surviving DVC sister cell or the supernumerary DVC neuroblast descendants. Only 4/28 embryos displayed a clear cell death in any cell by the end of the recording, including Caapap which is normally fated to die (Fig. S5). All lineaged *ham-1(n1438)* embryos displayed a single DVC neuron with Caapaa correctly adopting DVC fate 8/10 embryos, and Caapap doing so in 2/10. However, only 4/10 embryos displayed a *wild type* terminal division pattern in which Caapa does not divide precociously, Caapaa adopts DVC fate and Caapap undergoes apoptosis. Overall, the loss of apoptosis was also milder in *ham-1(n1438)* embryos with a cell death evident in 7/10 embryos (Fig. S6).

Having seen this effect on terminal fates, and the equalisation of preceding cleavages we asked whether the terminal division of Caapaa is also equalised in *pig-1(gm344)* mutants. Cell size at the terminal division provided a technical challenge to DIC image measurement. However, as nucleus size can be used as a proxy for overall cell size (Ginzberg et al., 2018), we took advantage of the fact that the *hlh-14::gfp [gmIs20]* reporter is both nuclear and expressed in *pig-1(gm344)* mutants. We find that the nuclear size ratio at the Caapaa cleavage displays an anterior bias in *wild type* embryos and that Caapap, fated to die, is smaller (Fig. 4D). This is significantly equalised in *pig-1(gm344)* mutants (Fig. 4D). Despite the DVC neuroblast itself being significantly enlarged due to the equalisation of the Caa and Caap divisions, the equalisation of the Caapa cleavage results in a similar sized nucleus in *pig-1(gm344)* mutants and *wild types* (Fig S2 and Fig S7).

Combined, this lineage and terminal division size ratio analyses demonstrates that both *pig-1* and *ham-1* play a role in the both the unequal cleavage of the DVC neuroblast and the correct acquisition of asymmetric terminal cell fates (neuron vs cell death).

**The Caap blastomere cleavage is affected in *hlh-14(tm295)* mutants**

The disruption of the unequal cleavages of Caa and Caap in *pig-1(gm344)* and *ham-1(n1438)* mutants has minimal impact on the expression of *hlh-14*. We therefore wondered what the purpose of these unequal cleavages may be and how they are regulated. We hypothesised that, given the lack of embryonic cell growth, these unequal cleavages may be regulated to control terminal cell size and speculated that they may therefore be under the control of the same factors that regulate cell fate acquisition. 4D-lineage analysis of *hlh-14(tm295)* null mutants revealed no defect in the Caa cleavage. In contrast, the unequal cleavage of Caap is strongly affected and resembles the hypoblast/hypoblast divisions of other C lineage branches (Fig. 5A,B and Fig. S2). Also, in agreement with previous work (Poole et al., 2011), 4D-lineaging confirmed that Caapa divides precociously in *hlh-14(tm295)* (Fig. 5C and Fig. S3). These results suggest that the proneural transcription factor HLH-14 acts to regulate the unequal cleavage and resultant daughter size asymmetry at the Caap division. In contrast, detected expression of the *hlh-14* transgenes only begins in the daughter cells themselves. However, close analysis of an *hlh-14 fosmid::gfp* transgene pattern and timing demonstrated two distinct phases of expression with the first detected as soon as 11 minutes post-division (Fig. S8). Given the maturation time and photostability of GFP (Balleza et al., 2018; Heppert et al., 2016), this early phase of expression is consistent with transcription of *hlh-14* in Caap, the mother of Caapa and Caapa.

***let-19* is an upstream regulator of *hlh-14* in the C lineage**

Reasoning that upstream regulators of *hlh-14* would exhibit a precocious division of the DVC neuroblast Caapa, we performed a 4D lineage-based screen of temperature sensitive, embryonic lethal mutants for such a phenotype. This screen revealed a mutant allele, *t3273*, which mapping-by-sequencing, complementation testing and rescue experiments reveal is an allele of the Mediator complex kinase module subunit LET-19 (Fig. S9; Materials and methods). Many of the Mediator complex subunits are ubiquitously expressed in *C. elegans* (Steimel et al., 2013; Wang et al., 2004; Zhang and Emmons, 2000) and we confirmed *let-19* expression in Caa, Caap and their descendants (Fig. S10).

Following identification, we characterised *let-19(t3273)* mutants together with a second *let-19* allele, *(t3200),* and assessed whether they shared additional phenotypes with *hlh-14* mutants, namely loss of both *hlh-14* expression and neuronal cell fates (Poole et al., 2011). In gastrulation stage *let-19(t3273)* mutants *hlh-14* expression was lost in the would-be DVC neuroblast Caapa in just over half of the lineaged embryos at the non-permissive temperature of 25°C, with a far higher penetrance observed in *let-19(t3200)* (Fig. 6A). Downstream of *hlh-14* expression, DVC cell fate was assessed using the transcriptional reporter for the unique DVC marker *ceh-63. let-19(t3200)* displayed a higher penetrance of loss with all embryos lacking *ceh-63* expression (Fig. 6B). A histone-RFP fusion driven by the promoter of hypodermal marker *dpy-7* was used to assess adoption of hypodermal (non-neural ectodermal) fate with *let-19(t3200)* again displaying a more highly penetrant phenotype. For both alleles it is unclear why the adoption of hypodermal fate in Caapaa displays a lower penetrance than that of the loss of the *hlh-14* expression. For *let-19(t3200),* a subset of the embryos analysed carried all three reporters at once which allowed concomitant assessment in the same embryo. In these embryos *ceh-63* expression was never detected in embryos lacking *hlh-14.* Conversely, *dpy-7* was only detected in those embryos lacking *hlh-14* expression (Fig. 6D). We also observed that *let-19* mutant animals display a very high degree of embryonic lethality (Fig. S9) and frequently fail to undergo morphogenesis. It is notable that in addition to a loss of *hlh-14* expression, Caapa occupies a lateral position in the posterior of the embryo at the C16 stage, contrasting the central position of the *wild type* cell (Fig. 6D). This is also the position of Caapa in *hlh-14* null mutants (Poole et al., 2011) further supporting the loss of neuronal cell fate and transformation to a hypoblast. All together this demonstrates that *let-19* is required for the correct specification of the DVC neuroblast.

### *let-19* regulates the unequal cleavage of the Caa and possibly Caap blastomeres

Taking advantage of the temperature sensitive nature of the *let-19* alleles we aimed to define the timing of action for LET-19 in the regulation of *hlh-14* expression and neurogenesis in the lineage. As the stronger and more consistent allele, assessment of this critical period was undertaken with *let-19(t3200).* Timed temperature shifts from both permissive to non-permissive (15°C to 25°C) temperatures and non-permissive to permissive (25°C to 15°C) and assessment of the loss of *ceh-63* expression in Caapaa (DVC) established that LET-19 acts around the time of the Caa cleavage (Fig. 6E). We find that in all *let-19(t3200)* embryos analysed, there is a striking equalisation of this cleavage (Fig. 7A-B). To quantify this equalisation a subset of the *let-19(t3200)* embryos

assessed for *hlh-14* expression in Fig. 6 were measured for cell volumes and all display a significant equalisation of the Caa cleavage ratio (Fig. 7B and Fig. S2A). Of the nine *let-19(t3273)* embryos scored for *hlh-14* expression in Caapa in Fig. 6, seven were measured for cell volumes. A further two embryos in which *hlh-14* expression was assessed in Caapaa instead (not included in Fig. 6), were also measured. This allowed the concordance between the presence or absence of *hlh-14* expression in the C lineage and cell volume ratios to be assessed in this second set of nine embryos. We find the Caa cleavage ratio is significantly equalised in those embryos lacking *hlh-14* expression (Fig 7B). We also observe defects in the unequal cleavage of Caap, particularly in *let-19(t3273)* embryos lacking *hlh-14* expression, which also show a significant equalisation of the cleavage. This is milder in *let-19(t3200)* mutants, where the cleavage mostly resembles the *wild type* (Fig. 7C).

We also quantified the division time of Caapa in both *let-19* mutants. Precocious division of Caapa was observed in all *let-19(t3200)* mutants regardless of *hlh-14* expression (Fig. 7D and Fig. S3). As with the cell volume ratio defects, precocious division of Caapa correlates with *hlh-14* expression in *let-19(t3273)* with those lacking *hlh-14* demonstrating a precocious Caapa division (Fig. 7D and Fig. S3). In addition, a highly variable extra division phenotype was observed in various branches of the C lineage affecting 3/9 *let-19(t3273)* embryos; 1/5 *let-19(t3273)* of those expressing *hlh-14* and 2/4 lacking *hlh-14* expression (Fig. 7D). In addition to its role as an upstream regulator of *hlh-14* expression and therefore the acquisition of neural fate, these results suggest *let-19* strongly regulates the unequal cleavage of Caa, and more weakly that of Caap, thereby controlling the size of their daughters.

## Discussion

How cell size is specified during development, how cells sense size and the consequences of cell size on cell fate and function are fundamental questions in biology. Cell size can be regulated by either cell growth or the total number of divisions. It can also be more specifically regulated by the control of daughter cell size asymmetry during mitosis. Many asymmetric divisions that generate daughter cells of different fates are also unequal, generating daughter cells of different sizes. How and why this occurs during development is unclear. One possibility is that unequal cell size directly affects asymmetric cell fate decisions. A clear example of this is seen in the alga *Volvox carteri*,

where cleavage plane manipulation experiments results result in daughter cell fate defects (Kirk et al., 1993). However, in other contexts, such as the exit of pluripotency in the daughters of asymmetric embryonic stem cell divisions, cell size does not appear to play any role in cell fate decisions (Chaigne et al., 2020). The work presented in this study provides evidence that cell size alone, through unequal cleavage, does not play a major role in the expression of the proneural gene *hlh-14/ASCL1* and so the specification of DVC neuroblast fate. We can therefore conclude that in a variety of different contexts cell size does not affect certain aspects of cell fate specification.

We have shown here that *pig-1/MELK* regulates the unequal cleavage of Caa and Caap, and that Caap cleavage is also regulated by *ham-1/STOX*. These genes have been previously described to regulate the unequal cleavages of asymmetrically dividing *C. elegans* neuroblasts with a smaller daughter that dies, such as in the Q and NSM neuroblast (Cordes et al., 2006; Feng et al., 2013; Frank et al., 2005; Guenther and Garriga, 1996; Leung et al., 2016; Wei et al., 2017; Teuliere et al., 2018). Although *pig-1/MELK* has a redundant role in the unequal division of the 1-cell embryo and the EMS blastomere at the 4-cell stage (Liro et al., 2018; Morton et al., 2012; Pacquelet et al., 2015), to our knowledge this is the first example of it regulating successive divisions in a lineage. This is likely through one of two mechanisms employed in other *C. elegans* cleavages; asymmetric spindle positioning or control of cortical myosin distribution and contractility (Ou et al., 2010; Wei et al., 2020).

We see little effect on the expression of *hlh-14/ASCL1* in the DVC neuroblast, as a result of equalising either the Caa or Caap divisions in *pig-1* or *ham-1* mutants. Nor is *hlh-14* detected ectopically in a sister branch of an equalised cleavage. Indeed, the production of a DVC neuron is also not abolished in most *pig-1* or *ham-1* mutant embryos. Together this suggests that equalisation does not prevent correct DVC neuroblast specification and as such neural fate specification in this lineage. However, *pig-1(gm344)* clearly does affect the terminal division of the DVC neuroblast in a number of ways. As in previously investigated lineages, we find that PIG-1 regulates the unequal cleavage of the DVC neuroblast and disrupts the segregation of neuronal and apoptotic fate. This is evidenced by the reversal of the division and/or the inappropriate survival of the DVC sister cell normally fated to die and therefore the loss or duplication of DVC. Furthermore, *pig-1* mutants also display cell cycle defects such as the precocious and supernumerary divisions of the DVC neuroblast, providing a source of supernumerary DVC neurons. One intriguing possibility for future investigation is that the DVC blastomere can somehow sense that it is too large. This could then either lead

it to divide early, consistent with the power-law relationship previously described between cell size and cell cycle timing (Arata et al., 2014), or to even undergo an extra round of division as we observe in a small fraction of *pig-1* mutants. Consistent with this possibility we observe a trend in *pig-1* mutant animals in that the larger the DVC neuroblast is the more likely it is to undergo an extra division (Fig. S7).

Through a forward genetic screen we have identified the Mediator complex kinase module component *let-19/MDT13* as a regulator of neural specification in the C lineage. In *let-19* mutants, *hlh-14/ASCL1* expression is lost, the DVC neuroblast divides precociously and its daughters acquire a hypodermal cell fate. The Mediator complex is an evolutionarily conserved regulator of transcriptional events including those in *C. elegans* (Grants et al., 2015) and as our mutants are embryonic-lethal, C lineage neurogenesis is likely one of many molecular events affected by these alleles. However, their temperature-sensitive nature permitted identification of the critical period of action LET-19 in our case, around the time of the Caa division. Indeed, in addition to *let-19*, the three other kinase module components *dpy-22/MDT12*, *cdk-8/CDK8* and *cic-1/CCNC(Cyclin C),* have been implicated in specific cells during neuronal development in the worm (Doitsidou et al., 2018; Luo and Horvitz, 2017; Wang et al., 2004; Zhang and Emmons, 2000) and in asymmetric cell divisions more generally (Grants et al., 2016; Yoda et al., 2005). What is perhaps surprising is that we show here that *let-19* is also required for the unequal cleavage of Caa. This is to our knowledge the first account of *let-19* affecting an unequal cleavage. Furthermore, we find that *hlh-14/ASCL1* regulates the unequal cleavage of Caap, in addition to specifying DVC neuroblast cell fate. As an upstream regulator of *hlh-14* why do *let-19* mutants not phenocopy *hlh-14* mutants in terms of cleavage equalisation rather than affecting different cleavages? An explanation possibly lies in the two distinct phases of *hlh-14* expression in Caapa we observe (Fig. S8). The early phase is consistent with transcription of *hlh-14* in Caap, appearing as soon as 11 minutes post-division, LET-19 may only be required to regulate the second later phase of *hlh-14* in Caapa. Altogether our results allow us to conclude that two successive unequal divisions in the C lineage are regulated by key neural cell fate regulators to determine embryonic neuroblast cell size. This parallel regulation of the cellular (cell size) and molecular (neuronal fate) aspects has been described in *C. elegans* before. In the Q lineage the proneural factor *lin-32/ATONAL* affects both unequal cleavages and fate acquisition (Zhu et al., 2014). In this context, our results present a clear second example of proneural gene dependent regulation of

cell size and may therefore indicate a conserved principle in *C. elegans* in the regulation of cell size and fate acquisition in tandem by the same factors.

From a developmental perspective, the fact that the *C. elegans* embryo lacks cell growth and has an invariant cell lineage and a fixed number of cells puts potential constraints on the size of cells generated by equal cell cleavages (Sulston et al., 1983). With this lack of growth, the spatial arrangement and size of cells may require tight regulation to produce intact, functional tissues as the worm hatches. Recently this has been described in the *Ciona* embryonic tailbud where unequal cleavages producing cells of symmetric fate are required for correct morphogenesis (Winkley et al., 2019). From a functional perspective, cell types have defined sizes and morphologies linked to function (Ginzberg et al., 2015). The size of neuronal cell bodies is linked to neuronal function owing to its impact on ion channel density and action potential strength and efficiency (Sengupta et al., 2013). Neurons have the smallest soma of all *C. elegans* cells, born only after the 10th or 11th cleavage round in the AB or MS lineages (Sulston and Horvitz, 1977; Sulston et al., 1983). The C lineage produces large hypodermal cells and the small DVC neuron after the 8th cleavage. In the absence of a general cell growth or shrinking in the embryo, two unequal divisions appear to be an efficient solution for scaling cell size down to a small neuron. If this were the case one might expect that control of these unequal cleavages is linked to the acquisition of cell fate and this is exactly what we observe.

We have shown that, in addition to the overall topology of the C lineage, the two unequal cleavages of Caa and Caap are conserved over 20M years of *Caenorhabditis* evolution (this study; Zhao et al., 2008; Memar et al., 2019). It has been argued that the higher developmental rates observed in *Caenorhabditis* species, produced an evolutionary pressure towards generating cells in the correct position in the embryo, rather than relying on extensive cell migrations (Houthoofd et al., 2003). In support of this there is a greater degree of lineage monoclonality in more basal species (Schulze and Schierenberg 2011; Schulze and Schierenberg 2009; Schulze et al., 2012). Interestingly, while the C lineage is highly conserved in the distantly related Rhabditids *Pellioditis marina* and *Rhabditophanes sp.,* in the slower developing species *Halicephalobus gingivalis* it produces only hypodermal and muscle cells (Houthoofd et al., 2003; Houthoofd et al., 2008; Houthoofd and Borgonie 2007). The homologous neurons appear to be generated from the AB lineage, migrating to their final position in the posterior of the embryo (Houthoofd et al., 2003). It is therefore tempting to speculate that the constraints of rapid developmental timing and invariant lineage which produce

polyclonal neural fate specification may combine with the functional requirement for neurons to be small discussed above. This could therefore necessitate co-regulation of unequal cleavages and neuronal fate to efficiently control fate and cell size in a branch that only undergoes 8 cell cycles. All together our results lead to the proposal that the fate regulator-dependent control of cell size via unequal cleavage is a versatile molecular mechanism to generate cell size differences in the absence of cell growth and volume modulation.

## Materials and methods

### *C. elegans* strain procurement and maintenance

*C. elegans* strains used in this study were derived from the N2 reference strain and were maintained at 20°C, with temperature-sensitive strains maintained at 15°C in accordance with standard practice (Stiernagle, 2006). A number of strains were obtained from the *Caenorhabditis* Genetics Center, based at the University of Montana, USA (cgc.umn.edu). NG4280 was obtained from the National Bioresource Project for *C. elegans* housed at the Mitani Lab at the Tokyo Women's Medical University School of Medicine, Japan (shigen.nig.ac.jp/c.elegans/). Some strains were kind gifts from Oliver Hobert and Barbara Conradt.

### Microscopy and imaging

DIC (Nomarski) and fluorescent imaging was undertaken with a Zeiss Axio ImagerM.2 upright microscope (Carl Zeiss) using a 100x/1.3 oil immersion objective and mounted pco.sensicam or pco. edge 3.1 (PCO) sCMOS camera. For fluorescent imaging, illumination was controlled by either a Colibri.2 (Carl Zeiss) or Cool LED pE-2 (Cool LED) LED system. Image acquisition was controlled using the bespoke software, TimeToLive, (Caenotec, Prof. Ralf Schnabel, Börssum Germany). For DIC and fluorescent imaging, 4D lineage recording and phenotypic scoring embryos were mounted in the same manner. One or two cell embryos were collected by bisecting gravid hermaphrodites suspended in a drop of M9 buffer with a scalpel blade. Molten 2% agarose was flattened between glass microscope slides and the embryos placed on the resultant pad via mouth pipette. A coverslip was gently placed over the pad and M9 buffer introduced under to the pad for hydration. Melted petroleum jelly was used to seal the coverslip to the slide.

## 4D-Lineaging

4D-lineaging was performed as in (Schnabel et al., 1997). Image acquisition for 4D lineaging was achieved using a Zeiss Axio Imager.M2 microscope mounted with a pco. edge 3.1 sCMOS camera or a pco.sensicam (PCO Kelheim, Germany).. Recordings at the non-permissive temperature of 25°C consisted of 750 DIC Z-stacks acquired at 35 second intervals with 25 slices per stack at a spacing of 1 µm. Recordings at the permissive temperature of 15°C comprised 1500 scans owing to the slower pace of development. All parameters including scans using fluorescent channels were programmed for specific timepoints using the imaging software Caenotec. Manual lineaging was performed as described in (Schnabel et al., 1997) using the Simi BioCell software (Simi Reality Motion, Unterschleissheim, Germany) software. The microenvironment under the objective was kept at a constant temperature via either an F12-ED or CD-200F Refrigerated/Heating Circulator (Julabo, Seelbach, Germany) and a bespoke copper collar surrounding the 100x objective.

## Temperature shift experiments

Temperature shift experiments were conducted using the same setup as for temperature controlled 4D-lineaging described in the 4D-Lineaging section above. Temperature downshift recordings were started at the non-permissive temperature 25°C and the temperature of the heated water circulator was changed to 15°C for the downshift after a set duration. The opposite was true for upshifts, which began at the permissive temperature 15°C and were then changed to the non-permissive 25°C. Data points were fitted to a Boltzmann sigmoid curve. Here, ‘Bottom’ refers to he lowest value of the curve, ‘Top’ to the highest and ‘V50’ the middle of the curve.

$$Y = Bottom + \frac{(Top - Bottom)}{1 - exp(\frac{V50 - X}{Slope})}$$

*Eqn.1 Boltzmann sigmoid curve*

The temperature-sensitive period (Suzuki 1970) or *tcrit* (Hirsh and Vanderslice 1976) was defined as starting at the point on the downshift at which the percentage mutant phenotype first non-zero. The end was defined as the point on the upshift at which the percentage mutant phenotype first reaches zero.

**4D-Lineage based screen of embryonic lethal, temperature sensitive mutants**

A forward genetic screen employing EMS mutagenesis was performed in accordance with standard protocols (Brenner, 1974). Mutants which were temperature sensitive at 25°C and did not fail at the very earliest stages of embryogenesis constituted the secondary screening population. These embryos were manually 4D-lineaged as described in the 4D-Lineaging section above. Mutants of interest we identified as those which phenocopied the precocious Caapa division of *hlh-14* mutants, or otherwise displayed C lineage aberrations.

**Cell volume and area measurements**

Cell pseudo-volumes were calculated from measured cell areas in DIC z-stack images using the image processing software Fiji (Schindelin et al., 2012). Stacks were acquired from the 4D-lineaging setup. Areas were measured by tracing the extent of the cell in an image. The volume between slices of the z-stack was calculated as a truncated cone with the slices know to be spaced 1 µm apart. The radii were calculated from circles of equivalent volume to those measured cell areas. The volumes between slices were summed to approximate cell volume and volume ratios between daughter cells were always expressed with respect to that of the posterior daughter; for example, 1.5 (1.5:1 A:P) or 0.85 (0.85:1 A:P, equivalent to 1:1.18).

$$V = \frac{\pi}{3}(r_1^2 + r_1 r_2 + r_2^2)h$$

*Eqn.2 Volume of a truncated cone*

Cell nuclei areas were measured in Fiji using maximum intensity projections of GFP images of the *gmIs20[hlh-14prom::hlh-14::gfp]* transgene.

**Statistical analysis and genotypes**

Statistical analyses were preformed using Graphpad Prism or Microsoft Excel. Absolute cell volumes, cell volume ratios, division timing and cell cycle ratios were compared using ANOVA analysis in Graphpad Prism, as there were more than three groups compare and all group comparison were computed. As group sample sizes were fewer than 50, Tukey's HSD test was used in post-hoc testing and correction for multiple comparisons. Groups were compared using t-tests conducted in Microsoft Excel when only two groups were compared in such cases, with no repeated measures.

The *pig-1, ham-1* and *let-19* mutant genetic backgrounds of samples analysed for cell volumes and cell volume ratios included either *gmIs20 [hlh-14prom::hlh-14::gfp rol-6(+)] II* alone or in combination with *otIs458 [ceh-63prom::gfp] III; stIs10166 [dpy-7p::HIS-24::mCherry,unc-119(+)]*. Therefore, the *"wild type"* samples in such cases comprised a combination of these same transgene backgrounds. There is no significant difference between these backgrounds for the cell volume ratios analysed (Fig. S11). As the *hlh-14(tm295)* mutant did not carry the transgenes, N2 was used as the *"wild type"* control strain for *hlh-14(tm295)*.

When phenotypes were assessed in the same embryos, the disparity between sample sizes for each phenotype is explained as follows. Division timing data for all mutant and *wild type* samples was collected in backgrounds containing *gmIs20 [hlh-14prom::hlh-14::gfp rol-6(+)]* (with the exception of *hlh-14(tm295)* and N2). A subset of these embryos had appropriately timed imaging to assess *hlh-14* expression in Caapa (the DVC neuroblast), a further subset again had appropriate image quality to allow cell measure measurements. As such there is a decreasing sample size for these phenotypes from the same set of embryos.

**Mapping and whole-genome sequencing**

Genomic DNA preparation was performed using the Gentra Puregene Tissue Kit (Qiagen) in accordance with the manufacturers supplemental nematode protocol. Library preparation was performed by the UCL Genomics team at the UCL Great Ormond Street Institute of Child Health. Mapping of causal mutations was performed via the "Hawaiian Cross" mapping-by-sequencing method. Strains were crossed to the highly polymorphic Hawaiian CB4856 strain and linkage of N2 regions was used to locate the causal mutant locus (Doitsidou et al., 2016). Mutant genome analysis was performed using the Galaxy web server based (Afgan et al., 2018) pipeline, CloudMap (Minevich et al., 2012). The Galaxy server was maintained by R.J.P.

**Complementation and rescue of *let-19* alleles**

Complementation crosses were performed to confirm non-complementation of the *t3200* and *t3273* alleles. Further crosses confirmed non-complementation between *t3200* and another known *let-19* allele *t3219.* Non-complementation between *t3219* and the mnDf46 deficiency which covers only the *let-19* and *rol-6* genes, had confirmed *t3219* as a *let-19* allele. Either the GFP marker *ceh-63::gf* or *flp-10::gfp* was first crossed into the males so that cross progeny could be identified and only those scored for lethality. Crosses were

performed at 15°C in both directions so that males of each mutant were crossed to the hermaphrodites of the opposite genotype. Gravid hermaphrodites from complementation crosses were singled and incubated at 25°C so that F1 embryos developed at the non-permissive temperature. To investigate maternal effect, crosses were performed in the male manner with *wild types* and each of the mutants. Rescue of embryonic lethality for *t3200* and *t3273* was performed using the WRM061cD04 fosmid, covering the region including the *let-19* locus and six further genes, three pseudo genes and a non-coding RNA. The sequence for WRM061cD04 is publicly available from the nematode research community database (wormbase.org/species/c_elegans/sequence/WRM061cD04). Mutant strains containing the fosmid as an extrachromosomal array fused to *myo-2::gfp* were built. P0s were singled to 25°C and lethality was scored for F1 embryos with or without the array; presence was indicated by GFP.

**Image processing**

Imaging data, including Z-stack construction and maximum intensity projections were processed using Fiji, a distribution of ImageJ (Schindelin et al., 2012).

**Strain list – *C. elegans***

| **Strain Number** | **Genotype** |
|---|---|
| CB4856 | *Hawaiian* |
| CHL5 | *otIs458[ceh-63prom::gfp] III; otIs92[flp-10prom::gfp]* |
| CHL28 | *stIs10166 [dpy-7p::HIS-24::mCherry + unc-119(+)]; let-19(t3200) gmIs20 [hlh-14prom::hlh-14::gfp rol-6(+)] II; otIs458 [ceh-63::gfp] III* |
| CHL22 | *let-19(t3200) gmIs20 [hlh-14prom::hlh-14::gfp rol-6(+)] II* |
| CHL31 | *stIs10166 [dpy-7p::HIS-24::mCherry + unc-119(+)]; gmIs20 [hlh-14prom::hlh-14::gfp rol-6(+)] II; otIs458 [ceh-63::gfp] III* |
| CHL40 | *let-19(t3273); drpEx1[WRM061Cd04, myo-2 prom::gfp rd 2.3.2 (line1)* |
| CHL41 | *let-19(t3273); drpEx2[WRM061Cd04, myo-2 prom::gfp rd 4.3.1* |

| | |
|---|---|
| | *(line2)* |
| CHL42 | *let-19(t3273); drpEx3[WRM061cD04, myo-2 prom::gfp rd 3.1 (line3)* |
| CHL51 | *gmIs20 [hlh-14prom::hlh-14::gfp rol-6(+)] II; otIs458 [ceh-63::gfp] III; pig-1(gm344) IV* |
| CHL52 | *stIs10166 [dpy-7p::HIS-24::mCherry + unc-119(+)]; gmIs20 [hlh-14prom::hlh-14::gfp rol-6(+)] II; otIs458 [ceh-63::gfp] III, pig-1(gm344) IV* |
| CHL53 | *stIs10166 [dpy-7p::HIS-24::mCherry + unc-119(+)]; gmIs20 [hlh-14prom::hlh-14::gfp rol-6(+)] II; otIs458 [ceh-63::gfp] III; ham-1(n1438) IV* |
| CHL54 | *let-19(t3273) II gmIs20 [hlh-14prom::hlh-14::gfp rol-6(+)] II* |
| CHL55 | *let-19(t3273) II; otIs458 [ceh-63::gfp] III* |
| GE4421 | *let-19(t3200) II* |
| GE4547 | *let-19(t3219) II* |
| HS616 | *osEx108 [(pAY105) let-19::GFP + rol-6(su1006)]* |
| GE4634 | *let-19(t3273) II* |
| MD3998 | *bcSi43[pig-1::gfp] II; unc-119(ed3) III* |
| MT3351 | *ham-1(n1438) IV* |
| N2 | *wild type* |
| NG4080 | *gmIs20 [hlh-14prom::hlh-14::gfp rol-6(+)] II* |
| NG4280 | *hlh-14(tm295)/mln1 II [mIs14 dpy-10(e128)]* |
| OH10173 | *Ex[hlh-14FOS(WRM0627dH07)::yfp; rol-6(d)]* |
| OH11974 | *otIs458 [ceh-63::gfp] III* |
| SD1546 | *stIs10166 [dpy-7p::HIS-24::mCherry + unc-119(+)]* |

| | |
|---|---|
| SP582 | *unc-4(e120) mnDf46/mnC1 dpy-10(e128) unc-52 (e444)II* |
| MD3876 | *pig-1(gm344) IV* |
| MD3877 | *pig-1(tm1510) IV* |
| CHL17 | *stIs10166 [dpy-7p::HIS-24::mCherry + unc-119(+)]; let-19(t3273) II* |
| OH15657 | *otIs713[hlh-14 fosmid::gfp; ttx-3 prom::rfp]* |
| CHL154 | *pig-1(gm344) IV; otIs713[hlh-14 fosmid::gfp; ttx-3 prom::rfp]* |
| CHL155 | *pig-1(tm1510) IV; otIs713[hlh-14 fosmid::gfp; ttx-3 prom::rfp]* |

**Strain list – other *Caenorhabditis* species**

| **Strain number** | **Genotype** |
|---|---|
| AF16 | *C. briggsae* |
| CB5161 | *C. brenneri* |
| EM646 | *C. remanei ssp. vulgaris* |

**Acknowledgements**

This work was supported by a Wellcome Senior Research Fellowship (207483/Z/17/Z) and a BBSRC Responsive Mode Grant (BB/X00208X/1) to R.J.P. and a Wellcome Four-Year PhD studentship to T.W.M (105380/Z/14/Z). We thank Cathrin Struck and Katharina Luthe for their work on the non-complementation of *t3200/t3219* and *t3219/mnDf46* respectively. We thank the Hobert lab, Conradt lab, CGC (Minnesota, USA) and NBRP (Tokyo, Japan) for strains. We thank Barbara Conradt, Nate Goehring and members of the Poole lab for critical reading of the manuscript and Sheila Poole for help editing the manuscript.

## References


**Arata, Y., Takagi, H., Sako, Y. and Sawa, H.** (2014). Power law relationship between cell cycle duration and cell volume in the early embryonic development of Caenorhabditis elegans. *Front Physiol* **5**, 529.

**Balleza, E., Kim, J. M. and Cluzel, P.** (2018). Systematic characterization of maturation time of fluorescent proteins in living cells. *Nat. Methods* **15**, 47–51.

**Bonaccorsi, S., Giansanti, M. G. and Gatti, M.** (2000). Spindle assembly in Drosophila neuroblasts and ganglion mother cells. *Nat Cell Biol* **2**, 54–56.

**Boveri, T.** (1899). Die Entwickelung von Ascaris megalocephala mit besonderer Rücksicht auf die Kernverhältnisse / von Theodor Boveri.

**Bowman, S. K., Neumüller, R. A., Novatchkova, M., Du, Q. and Knoblich, J. A.** (2006). The Drosophila NuMA Homolog Mud Regulates Spindle Orientation in Asymmetric Cell Division. *Dev Cell* **10**, 731–742.

**Cabernard, C. and Doe, C. Q.** (2009). Apical/Basal Spindle Orientation Is Required for Neuroblast Homeostasis and Neuronal Differentiation in Drosophila. *Dev Cell* **17**, 134–141.

**Cabernard, C., Prehoda, K. E. and Doe, C. Q.** (2010). A spindle-independent cleavage furrow positioning pathway. *Nature* **467**, 91–94.

**Chaigne, A., Labouesse, C., White, I. J., Agnew, M., Hannezo, E., Chalut, K. J. and Paluch, E. K.** (2020). Abscission Couples Cell Division to Embryonic Stem Cell Fate. *Dev Cell* **55**, 195-208.e5.

**Colombo, K., Grill, S. W., Kimple, R. J., Willard, F. S., Siderovski, D. P. and Gönczy, P.** (2003). Translation of Polarity Cues into Asymmetric Spindle Positioning in Caenorhabditis elegans Embryos. *Science* **300**, 1957–1961.

**Conklin, E. G.** (1905). The organization and cell-lineage of the ascidian egg / by Edwin G. Conklin.

**Cordes, S., Frank, C. A. and Garriga, G.** (2006). The C. elegans MELK ortholog PIG-1 regulates cell size asymmetry and daughter cell fate in asymmetric neuroblast divisions. *Development* **133**, 2747–2756.

**Doe, C. Q., Chu-LaGraff, Q., Wright, D. M. and Scott, M. P.** (1991). The prospero gene specifies cell fates in the drosophila central nervous system. *Cell* **65**, 451–464.

**Doitsidou, M., Minevich, G., Kroll, J. R., Soete, G., Gowtham, S., Korswagen, H. C., Zon, J. S. van and Hobert, O.** (2018). A Caenorhabditis elegansZinc Finger Transcription Factor, ztf-6, Required for the Specification of a Dopamine Neuron-Producing Lineage. *G3 Genes Genomes Genetics* **8**, 17 26.

**Feng, H., Reece-Hoyes, J. S., Walhout, A. J. M. and Hope, I. A.** (2012). A regulatory cascade of three transcription factors in a single specific neuron, DVC, in Caenorhabditis elegans. *Gene* **494**, 73 84.

**Feng, G., Yi, P., Yang, Y., Chai, Y., Tian, D., Zhu, Z., Liu, J., Zhou, F., Cheng, Z., Wang, X., et al.** (2013). Developmental stage-dependent transcriptional regulatory pathways control neuroblast lineage progression. *Development* **140**, 3838 3847.

**Fickentscher, R. and Weiss, M.** (2017) Physical determinants of asymmetric cell divisions in the early development of *Caenorhabditis elegans. Sci Rep,* **7**, 9369.

**Frank, C. A., Hawkins, N. C., Guenther, C., Horvitz, H. R. and Garriga, G.** (2005). C. elegans HAM-1 positions the cleavage plane and regulates apoptosis in asymmetric neuroblast divisions. *Dev Biol* **284**, 301 310.

**Fuse, N., Hisata, K., Katzen, A. L. and Matsuzaki, F.** (2003). Heterotrimeric G Proteins Regulate Daughter Cell Size Asymmetry in Drosophila Neuroblast Divisions. *Curr Biol* **13**, 947 954.

**Ginzberg, M. B., Kafri, R. and Kirschner, M. W.** (2015). On being the right (cell) size. *Science* **348**, 1245075–1245075.

**Ginzberg, M. B., Chang, N., D'Souza, H., Patel, N., Kafri, R. and Kirschner, M. W. (2018)** Cell size sensing in animal cells coordinates anabolic growth rates and cell cycle progression to maintain cell size uniformity. *eLife,* **7**: e26957

**Gönczy, P.** (2008). Mechanisms of asymmetric cell division: flies and worms pave the way. *Nat Rev Mol Cell Bio* **9**, 355 366.

**Grants, J. M., Goh, G. Y. S. and Taubert, S.** (2015). The Mediator complex of Caenorhabditis elegans: insights into the developmental and physiological roles of a conserved transcriptional coregulator. *Nucleic Acids Res* **43**, 2442 2453.

**Grants, J. M., Ying, L. T. L., Yoda, A., You, C. C., Okano, H., Sawa, H. and Taubert, S.** (2016). The Mediator Kinase Module Restrains Epidermal Growth Factor Receptor Signaling and Represses Vulval Cell Fate Specification in Caenorhabditis elegans. *Genetics* **202**, 583 599.

**Grill, S. W., Gönczy, P., Stelzer, E. H. K. and Hyman, A. A.** (2001). Polarity controls forces governing asymmetric spindle positioning in the Caenorhabditis elegans embryo. *Nature* **409**, 630–633.

**Guenther, C. and Garriga, G.** (1996). Asymmetric distribution of the C. elegans HAM-1 protein in neuroblasts enables daughter cells to adopt distinct fates. *Development (Cambridge, England)* **122**, 3509 3518.

**Heppert, J. K., Dickinson, D. J., Pani, A. M., Higgins, C. D., Steward, A., Ahringer, J., Kuhn, J. R. and Goldstein, B.** (2016) Comparative assessment of fluorescent proteins for in vivo imaging in an animal model system. *Mol Biol Cell,* **7,** 27(22):3385-3394.

**Hirsh, D., & Vanderslice, R. (1976).** Temperature-sensitive developmental mutants of *Caenorhabditis elegans*. *Developmental Biology*, **49,** 220–235.

**Horvitz, H. R. and Herskowitz, I.** (1992). Mechanisms of asymmetric cell division: two Bs or not two Bs, that is the question. *Cell* **68**, 237 255.

**Houthoofd, W., Jacobsen, K., Mertens, C., Vangestel, S., Coomans, A. and Borgonie, G.** (2003) Embryonic cell lineage of the marine nematode *Pellioditis marina. Dev Biol* **258**, 57-69.

**Houthoofd, W. and Borgonie, G.** (2007) The embryonic cell lineage of the nematode *Halicephalobus gingivalis* (Nematoda: Cephalobina: Panagrolaimoidea). *Nematology* **9**, 573-584.

**Houthoofd, W., Willems, M., Jacobsen, K., Coomans, A. and Borgonie, G.** (2008) The embryonic cell lineage of the nematode *Rhabditophanes sp. Int J Dev Biol* **52**, 963-7.

**Jankele, R., Jelier, R. and Gönczy, P.** (2021). Physically asymmetric division of the C. elegans zygote ensures invariably successful embryogenesis. *eLife* **10**, e61714.

**Kirk, M. M., Ransick, A., McRae, S. E. and Kirk, D. L.** (1993). The relationship between cell size and cell fate in Volvox carteri. *J Cell Biology* **123**, 191–208.

**Knoblich, J. A.** (2008). Mechanisms of asymmetric stem cell division. *Cell* **132**, 583-597.

**Leung, A., Hua, K., Ramachandran, P., Hingwing, K., Wu, M., Koh, P. L. and Hawkins, N.** (2016). C. elegans HAM-1 functions in the nucleus to regulate asymmetric neuroblast division. *Dev Biol* **410**, 56-69.

**Liro, M. J., Morton, D. G. and Rose, L. S.** (2018). The kinases PIG-1 and PAR-1 act in redundant pathways to regulate asymmetric division in the EMS blastomere of C. elegans. *Dev Biol* **444**, 9–19.

**Loyer, N. and Januschke, J.** (2020). Where does asymmetry come from? Illustrating principles of polarity and asymmetry establishment in Drosophila neuroblasts. *Curr Opin Cell Biol* **62**, 70–77.

**Luo, S. and Horvitz, H. R.** (2017). The CDK8 Complex and Proneural Proteins Together Drive Neurogenesis from a Mesodermal Lineage. *Curr Biol* **27**, 661 672.

**Memar, N., Schiemann, S., Hennig, C., Findeis, D., Conradt, B. and Schnabel, R.** (2019) Twenty million years of evolution: The embryogenesis of four Caenorhabditis species are indistinguishable despite extensive genome divergence. *Dev Biol* **447**, 182-199.

**Morton, D. G., Hoose, W. A. and Kemphues, K. J.** (2012). A Genome-Wide RNAi Screen for Enhancers of par Mutants Reveals New Contributors to Early Embryonic Polarity in Caenorhabditis elegans. *Genetics* **192**, 929–942.

**Neumüller, R. A. and Knoblich, J. A.** (2009). Dividing cellular asymmetry: asymmetric cell division and its implications for stem cells and cancer. *Gene Dev* **23**, 2675–2699.

**Nguyen-Ngoc, T., Afshar, K. and Gönczy, P.** (2007). Coupling of cortical dynein and Gα proteins mediates spindle positioning in Caenorhabditis elegans. *Nat Cell Biol* **9**, 1294–1302.

**O'Farrell, P.** (2004). How Metazoans Reach Their Full Size: The Natural History of Bigness. *Cell Growth: Control of Cell Size (CSH Monograph)* **42**, 1–22.

**Ou, G., Stuurman, N., D'Ambrosio, M. and Vale, R. D.** (2010). Polarized Myosin Produces Unequal-Size Daughters During Asymmetric Cell Division. *Science* **330**, 677–680.

**Pacquelet, A., Uhart, P., Tassan, J.-P. and Michaux, G.** (2015). PAR-4 and anillin regulate myosin to coordinate spindle and furrow position during asymmetric division. *J Cell Biol* **210**, 1085–1099.

**Pham, T. T., Monnard, A., Helenius, J., Lund, E., Lee, N., Müller, D. J. and Cabernard, C.** (2019). Spatiotemporally Controlled Myosin Relocalization and Internal Pressure Generate Sibling Cell Size Asymmetry. *Iscience* **13**, 9–19.

**Poole, R. J., Bashllari, E., Cochella, L., Flowers, E. B. and Hobert, O.** (2011). A Genome-Wide RNAi Screen for Factors Involved in Neuronal Specification in Caenorhabditis elegans. *Plos Genet* **7**, e1002109.

**Rose, L. and Gönczy, P.** (2014). Polarity establishment, asymmetric division and segregation of fate determinants in early C. elegans embryos. *Wormbook* 1 43.

**Roubinet, C., Tsankova, A., Pham, T. T., Monnard, A., Caussinus, E., Affolter, M. and Cabernard, C.** (2017). Spatio-temporally separated cortical flows and spindle geometry establish physical asymmetry in fly neural stem cells. *Nat Commun* **8**, 1383.

**Schnabel, R., Hutter, H., Moerman, D. and Schnabel, H.** (1997). Assessing normal embryogenesis in *Caenorhabditis elegans* using a 4D microscope: variability of development and regional specification. *Dev Biol* **15**, 234-65.

**Schnabel, R., Bischoff, M., Hintze, A., Schulz, A. K., Hejnol, A., Meinhardt, H and Hutter, H.** (2006). Global cell sorting in the *C. elegans* embryo defines a new mechanism for pattern formation*. Dev Biol,* **5;294(2):** 418-31.

**Schindelin, J., Arganda-Carreras, I., Frise, E., Kaynig, V., Longair, M., Pietzsch, T., Preibisch, S., Rueden, C., Saalfeld, S., Schmid, B., Tinevez, J. Y., White, D. J., Hartenstein, V., Eliceiri, K., Tomancak, P and Cardona, A.** (2012). Fiji: an open-source platform for biological-image analysis. *Nat Methods* **28**, 676-82.

**Schulze, J. and Schierenberg, E.** (2009) Embryogenesis of *Romanomermis culicivorax:* an alternative way to construct a nematode. *Dev Biol* **334**, 10-21.

**Schulze, J. and Schierenberg, E.** (2011) Evolution of embryonic development in nematodes. *Evodevo* **2**, 18.

**Schulze, J., Houthoofd, W., Uenk, J., Vangestel, S. and Schierenberg, E.** (2012) Plectus - a stepping stone in embryonic cell lineage evolution of nematodes. *Evodevo* **3**, 13.

**Sengupta, B., Faisal, A. A., Laughlin, S. B. and Niven, J. E.** (2013). The effect of cell size and channel density on neuronal information encoding and energy efficiency. *J Cereb Blood Flow Metabolism* **33**, 1465–1473.

**Siller, K. H., Cabernard, C. and Doe, C. Q.** (2006). The NuMA-related Mud protein binds Pins and regulates spindle orientation in Drosophila neuroblasts. *Nat Cell Biol* **8**, 594–600.

**Srinivasan, D. G., Fisk, R. M., Xu, H. and Heuvel, S. van den** (2003). A complex of LIN-5 and GPR proteins regulates G protein signaling and spindle function in C. elegans. *Gene Dev* **17**, 1225–1239.

**Sulston, J. E., Schierenberg, E., White, J. G. and Thomson, J. N.** (1983). The embryonic cell lineage of the nematode Caenorhabditis elegans. *Developmental biology* **100**, 64 119.

**Sunchu, B. and Cabernard, C.** (2020). Principles and mechanisms of asymmetric cell division. *Development* **147**, dev167650.

**Suzuki, D. T.** (1970). Temperature-Sensitive Mutations in *Drosophila melanogaster*. *Science*, **170,** 3959.

**Teuliere, J., Kovacevic, I., Bao, Z. and Garriga, G.** (2018). The Caenorhabditis elegans gene ham-1 regulates daughter cell size asymmetry primarily in divisions that produce a small anterior daughter cell. *Plos One* **13**, e0195855.

**Tsankova, A., Pham, T. T., Garcia, D. S., Otte, F. and Cabernard, C.** (2017). Cell Polarity Regulates Biased Myosin Activity and Dynamics during Asymmetric Cell Division via Drosophila Rho Kinase and Protein Kinase N. *Dev. Cell* **42**, 143-155.e5.

**Wang, J.-C., Walker, A., Blackwell, T. K. and Yamamoto, K. R.** (2004). The Caenorhabditis elegans Ortholog of TRAP240, CeTRAP240/let-19, Selectively Modulates Gene Expression and Is Essential for Embryogenesis*. *J Biol Chem* **279**, 29270–29277.

**Wei, H., Yan, B., Gagneur, J. and Conradt, B.** (2017). Caenorhabditis elegans CES-1 Snail Represses pig-1 MELK Expression To Control Asymmetric Cell Division. *Genetics* **206**, 2069-2084.

**Wei, H., Lambie, E. J., Osório, D. S., Carvalho, A. X. and Conradt, B.** (2020). PIG-1 MELK-dependent phosphorylation of nonmuscle myosin II promotes apoptosis through CES-1 Snail partitioning. *Plos Genet* **16**, e1008912.

**Whitman, C. O.** (1878). Memoirs: The Embryology of Clepsine. *J Cell Sci* **s2-18**, 215–315.

**Winkley, K., Ward, S., Reeves, W. and Veeman, M.** (2019). Iterative and Complex Asymmetric Divisions Control Cell Volume Differences in Ciona Notochord Tapering. *Curr Biol*.

**Yoda, A., Kouike, H., Okano, H. and Sawa, H.** (2005). Components of the transcriptional Mediator complex are required for asymmetric cell division in C. elegans. *Development* **132**, 1885 1893.

**Zhang, H. and Emmons, S. W.** (2000). A C. elegans mediator protein confers regulatory selectivity on lineage-specific expression of a transcription factor gene. *Gene Dev* **14**, 2161–2172.

**Zhao, Z., Boyle, T. J., Bao, Z., Murray, J. I., Mericle, B. and Waterson, R. H.** (2008) Comparative analysis of embryonic cell lineage between *Caenorhabditis briggsae* and *Caenorhabditis elegans. Dev Biol* **314**, 93-99.

**Zhu, Z., Liu, J., Yi, P., Tian, D., Chai, Y., Li, W. and Ou, G.** (2014). A proneural gene controls C. elegans neuroblast asymmetric division and migration. *Febs Lett* **588**, 1136 1143.

# Figures

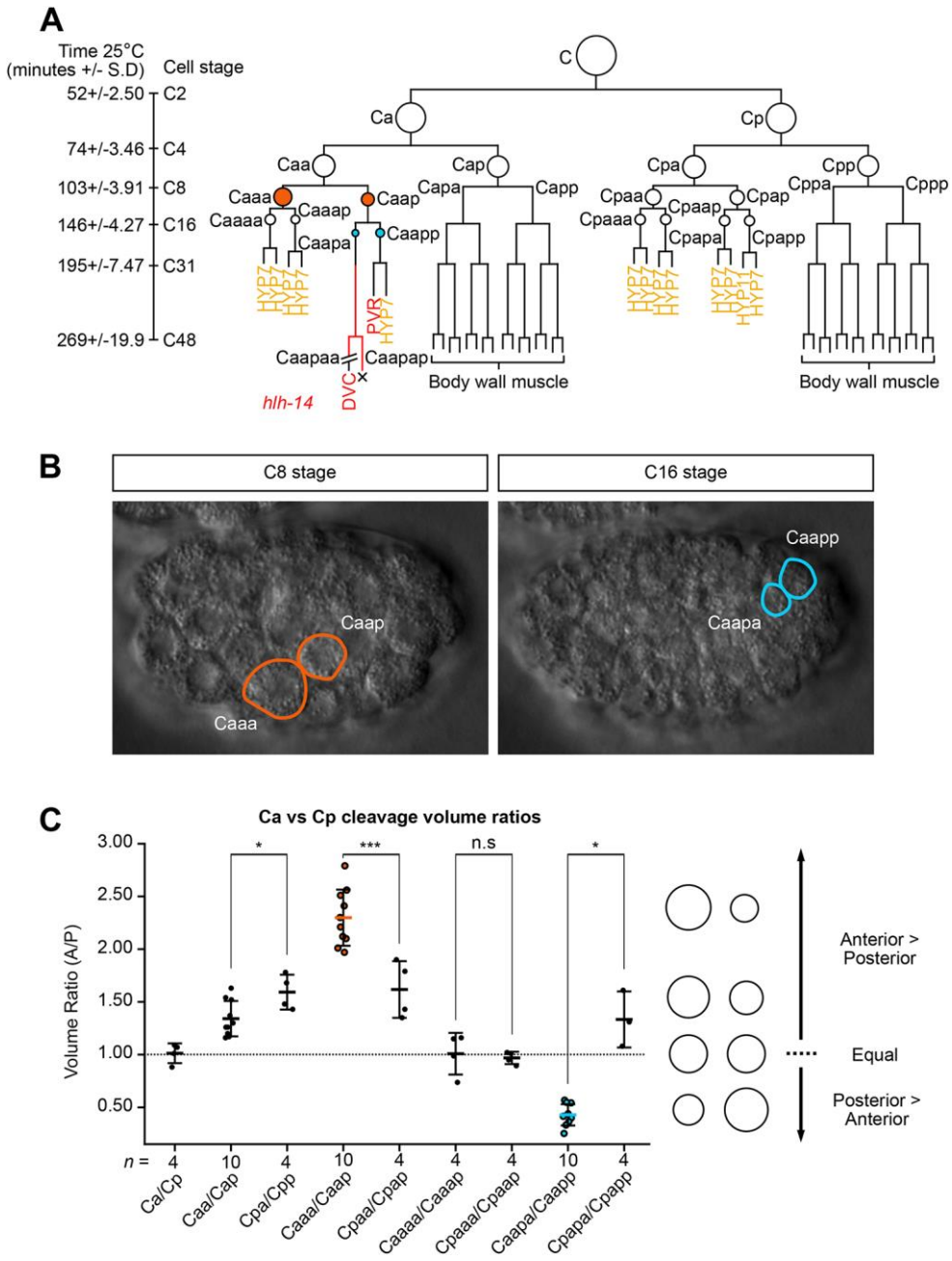


**Fig. 1. Two dramatically unequal cleavages precede *hlh-14* Expression in the C lineage**

(A) Lineage diagram of the C lineage. Branch lengths indicate division timings, circles indicate relative cell size. Caa daughters are indicated in orange, Caap daughters in blue. Red lines indicate the timing of *hlh-14 [gmIs20]* expression. Red letters indicate neuronal fate, yellow letters indicate hypodermal fate. Fading of *hlh-14* prior to terminal fate differentiation is indicated. Division timing at 25°C is indicated in minutes ± S.D, developmental stage of the C lineage expressed as total C lineage cell number. (B) DIC

images of *wild type* embryos representing the relative daughter cell sizes in the Caa and Caap cleavages. Length of a *C. elegans* embryo ~50µm. (C) Dot plot of the volumetric ratio of C lineage cleavages, expressed as the anterior/posterior daughter volume; with means and S.D. The dotted line indicates an equal cleavage ratio of 1:1. The same colour code as in A indicates the same divisions in B and C, Caa in orange, Caap in blue. Circles represent sister cell sizes at adjacent volume ratios. t-tests: n.s = not significant, * = $p<0.5$, *** = $p<0.001$.

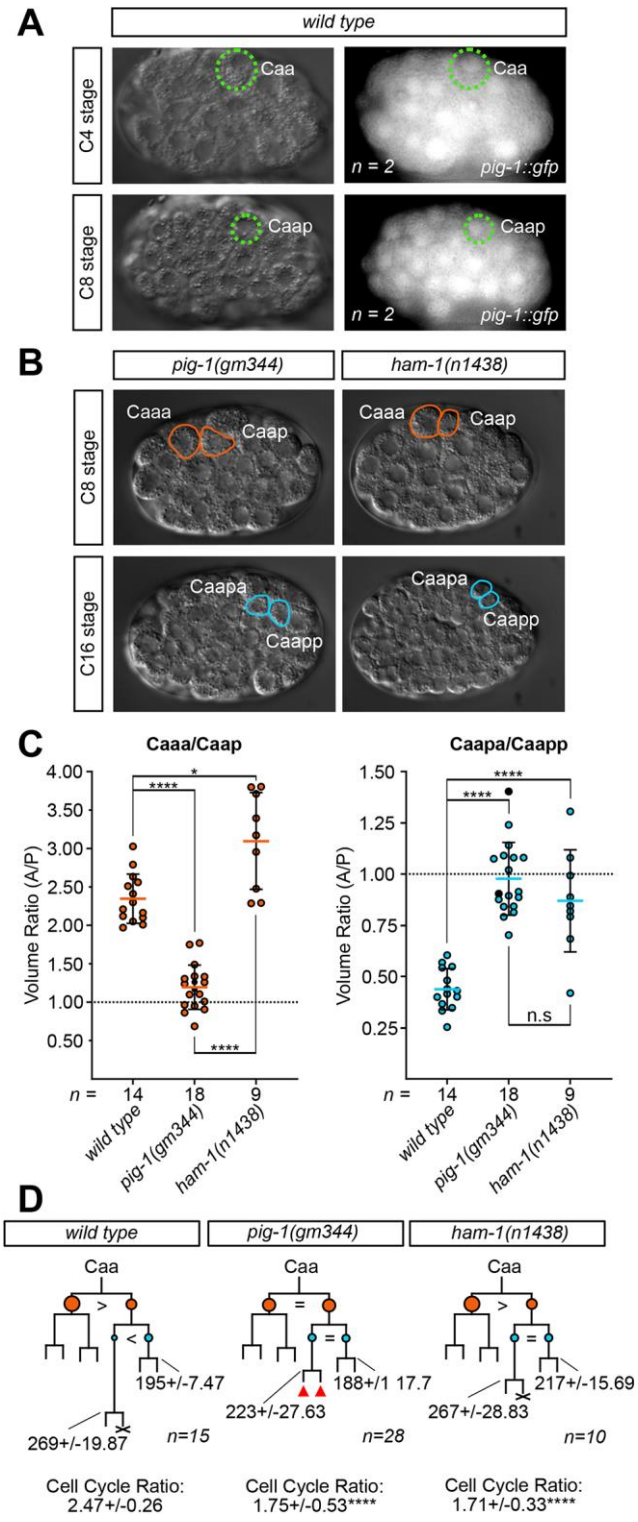


**Fig. 2. C lineage unequal cleavages are equalised in *pig-1(gm344) and ham-1(n1438)* mutants**

(A) DIC and GFP images, and lineage diagram indicating the expression of *pig-1 [bcSi43]* in *wild type* embryos in Caa and Caap. Length of a *C. elegans* embryo ~50µm. (B) DIC images presenting the unequal cleavages of Caa and Caap in *pig-1(gm344)* and *ham-1(n1438)* embryos. (C) Dot plot of the volumetric ratio of the Caa and Caap cleavages in

*wild type, pig-1(gm344)* and *ham-1(n1438)* embryos, expressed as the anterior/posterior daughter volume, with means and S.D. Black dots in *pig-1(gm344)* indicate no *hlh-14* expression. ANOVA: n.s = not significant, * = p<0.05, **** = p<0.0001. (D) Lineage diagrams of the neurogenic branch of the C lineage in the same mutants, from manually 4D-lineaged embryos. Branch lengths are indicative of division times. Circles indicate the relative sizes of cells. Caa daughters indicated in orange, Caap daughters in blue. = represents equal cleavages, > or < represents unequal cleavages.. Red triangle = extra divisions sometimes seen in branch, full details in Fig. S5. Caapa and Caapp division times represented in minutes ± S.D., with Cell Cycle Ratio of Caapa/Caapp expression ± S.D. Comparison to *wild type,* ANOVA: **** = p<0.0001. For details on *wild type* and mutant genotypes, refer to the materials and methods section.

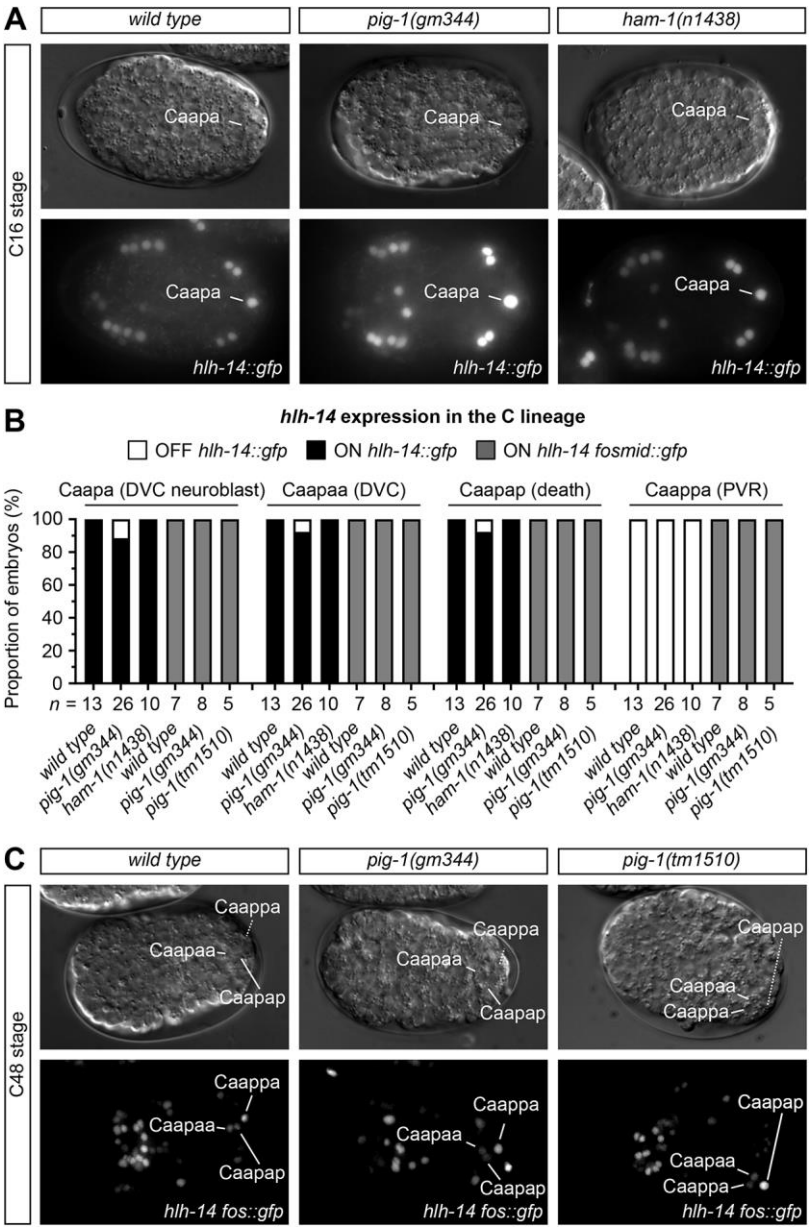


**Fig. 3. *hlh-14* expression in *pig-1(gm344)*, *pig-1(tm1510)* and *ham-1(n1438)* mutants**
(A) DIC images and GFP maximum intensity projections for *hlh-14* expression *[gmIs20]* in *wild type, pig-1(gm344)* and *ham-1(n1438)* bean-stage (gastrulation) embryos. Lines indicate expression in the DVC neuroblast Caapa. Length of a *C. elegans* embryo ~50µm. (B) Stacked bar chart of expression of *hlh-14 [gmIs20]* in the Caapa, Caapaa, Caapap and Caappa in *wild type, pig-1(gm344)* and *ham-1(n1438),* and of *hlh-14 [hlh-14 fosmid::gfp]* expression in *wild type, pig-1(gm344)* and *pig-1(tm1510)* lineaged embryos. *Wild type* fates of cells indicated in brackets. (C) DIC and GFP images of *hlh-14* expression *[hlh-14 fosmid::gfp]* in *pig-1(gm344)* and *pig-1(tm1510)* bean stage (gastrulation) embryos following terminal C lineage divisions. Representative of majority phenotypes. For details on *wild type* and mutant genotypes, refer to the materials and methods section.

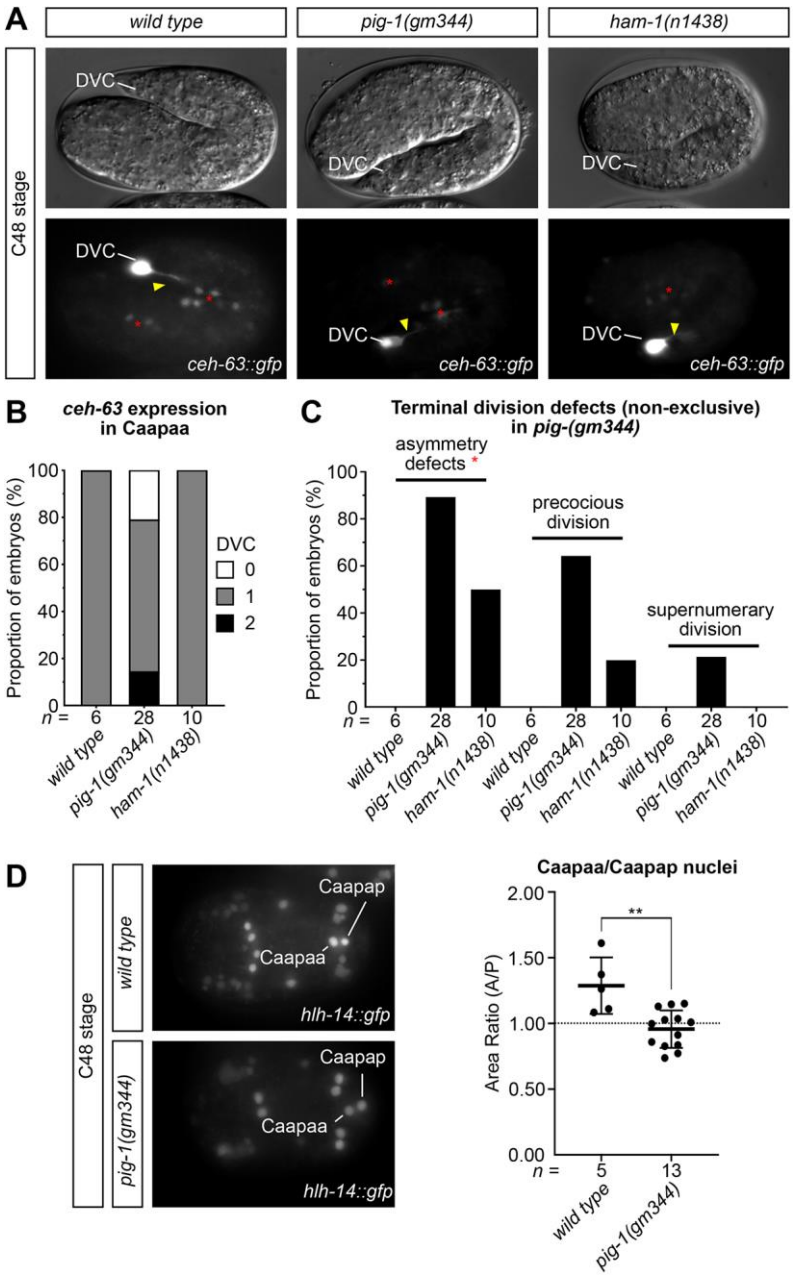


**Fig. 4. Terminal division defects in *pig-1(gm344)* and *ham-1(n1438)***

(A) DIC and GFP images for *ceh-63 [otIs458]* expression in *wild type, pig-1(gm344)* and *ham-1(n1438)* elongation stage embryos. DVC neuron indicated, yellow arrow = neuronal projection. Red star = residual *hlh-14* expression. Length of a *C. elegans* embryo ~50µm. (B) Stacked bar chart representing the number of *ceh-63* expressing cells *[otIs458]* at elongation stage in lineaged *pig-1(gm344)* and *ham-1(n1438)* embryos. (C) Bar chart representing terminal division phenotypes in lineaged *pig-1(gm344)* and *ham-1(n1438)* embryos. Categories are non-exclusive. Asymmetry defects = all non-*wild type* phenotypes, precocious division = precocious division of Caapa, supernumerary division = extra rounds of division of any Caapa daughter cells. (D) GFP maximum intensity projection images for *hlh-14 [gmIs20]* expression in lineaged *wild type* and *pig-1(gm344)*

embryos following Caapa division, indicating a loss of size asymmetry in *pig-1(gm344)* mutants. Cells indicated with lines. Dot plot of nuclear area ratio of the Caapa daughters in *wild type* and *pig-1(gm344))* embryos, expressed as the anterior/posterior daughter area, with means and S.D. t-test: ** = p<0.01. For details on *wild type* and mutant genotypes, refer to the materials and methods section.

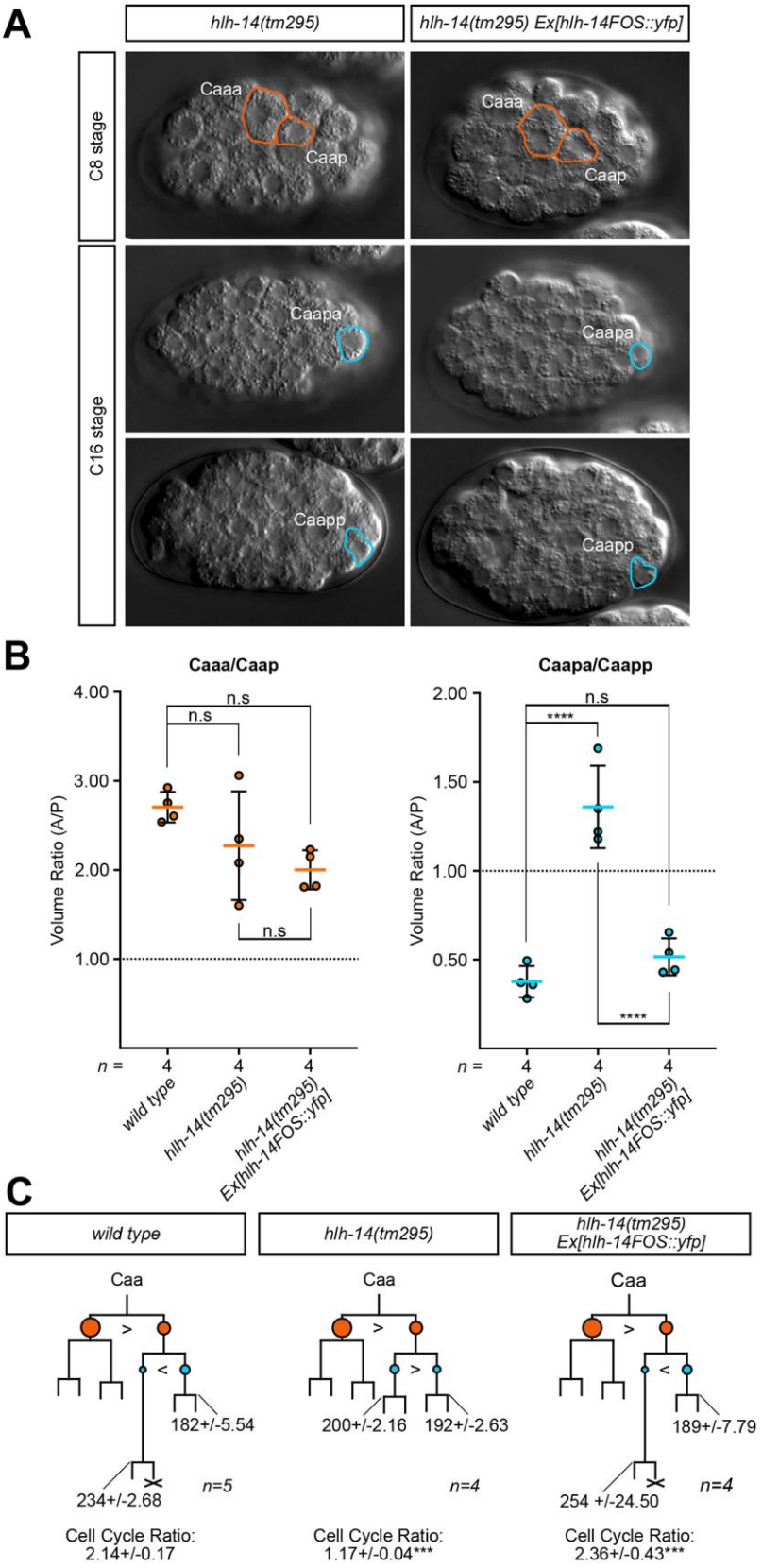


**Fig. 5. The Caap blastomere cleavage is affected in *hlh-14(tm295)* mutants**

(A) DIC images of *hlh-14(tm295)* and *hlh-14 fosmid* rescued embryos representing the relative daughter cell sizes at the Caa and Caap cleavages. Length of a *C. elegans* embryo ~50µm. (B) Dot plots of the volumetric ratio of the Caa and Caap cleavages in *wild*

*type* and *hlh-14(tm295)* embryos, expressed as the anterior/posterior daughter volume, with means and S.D. ANOVA: n.s = not significant, **** = p<0.0001. Dotted line indicates absolute equal cleavage ratio of 1:1. (C) Lineage diagrams of the neurogenic branch of the C lineage for *wild type, hlh-14(tm295)* and *hlh-14(tm295) fosmid* rescued embryos, constructed from manually 4D-lineaged embryos. Branch lengths are indicative of division timings. Circles represent relative sizes of cells; > or < representing the larger cell. Orange indicates Caa daughters, blue Caap daughters. Caapa and Caapp division times represented in minutes ± S.D., with Cell Cycle Ratio of Caapa/Caapp expression ± S.D. Comparison to *wild type,* ANOVA: *** = p<0.001. For details on *wild type* and mutant genotypes, refer to the materials and methods section.

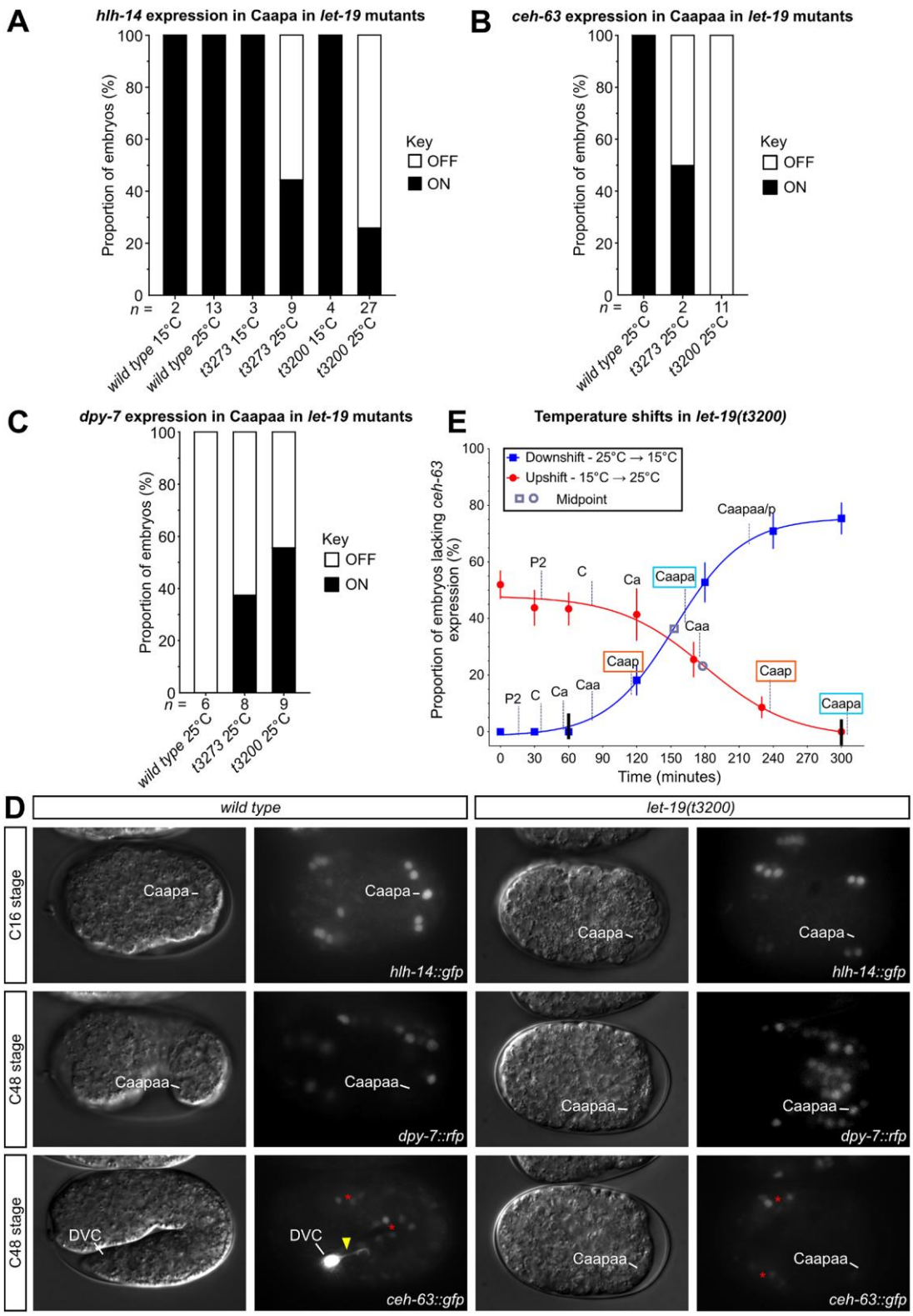


**Fig. 6. Loss of *hlh-14* expression and adoption of hypodermal fate in *let-19* mutants**

(A) Stacked bar chart for *hlh-14 [gmIs20]* expression in Caapa (DVC neuroblast) in lineaged *wild type, let-19(t3273)* and *let-19(t3200)* embryos at the permissive temperature 15°C and non-permissive temperature 25°C. *wild type* and *let-19(t3200)* embryos include embryos carrying only the *hlh-14 [gmIs20]* transgene or *hlh-14 [gmIs20], dpy-7 [stIs10166]*

and *ceh-63 [otIs458]* transgenes. *let-19(t3273)* embryos carried only *hlh-14 [gmIs20]*. (B) Stacked bar chart for *ceh-63 [otIs458]* expression in Caapaa in lineaged *wild type* and *let-19* mutant embryos, at non-permissive temperature 25°C. *wild type* and *let-19(t3200)* embryos include embryos carrying *hlh-14 [gmIs20], dpy-7 [stIs10166]* and *ceh-63 [otIs458]* transgenes. *let-19(t3273)* embryos carried only *ceh-63 [otIs458].* (C) Stacked bar chart for *dpy-7 [stIs10166]* expression in Caapaa in lineaged *wild type* and *let-19* mutant embryos, at non-permissive temperature 25°C. *wild type* and *let-19(t3200)* embryos include embryos carrying *hlh-14 [gmIs20], dpy-7 [stIs10166]* and *ceh-63 [otIs458]* transgenes. *let-19(t3273)* embryos carried only *dpy-7 [stIs10166].* (D) DIC and GFP maximum intensity projection images of *hlh-14* expression *[gmIs20]* in bean-stage (gastrulation), RFP images for *dpy-7 [stIs10166]* in later bean-stage (morphogenesis) and GFP images *ceh-63 [otIs458]* in one-fold (elongation) stage *wild type* and *let-19(t3200)* embryos carrying all three reporters. Mutant phenotypes are represented. Lines indicate the position of the Caapa (DVC neuroblast) or Caapaa (DVC in *wild type*). Red star = residual *hlh-14* expression in *ceh-63* images. Length of a *C. elegans* embryo ~50µm. (E) Percentage loss of *ceh-63* expression (DVC) curves in *let-19(t3200)* for upshifts from permissive to non-permissive temperature (15°C → 25°C) are plotted in red with downshifts in blue (25°C → 15°C). Black lines indicate the window of critical timepoint for LET-19 action. A grey square or circle indicates the mid-point of up and down shift curves respectively. Cell names are represented at birth times at each temperature condition on the relevant curve. X-axis represents timepoints for the temperature shift. The birth of Caap is indicated by an orange box, Caapa in blue. *n* = 40-60 for each timepoint in the downshift experiments (except n = *9,* 0 mins). *n* = 50-70 per timepoint for upshifts (except *n* = 102 at 0 mins, *n* = 29 at 120 mins).

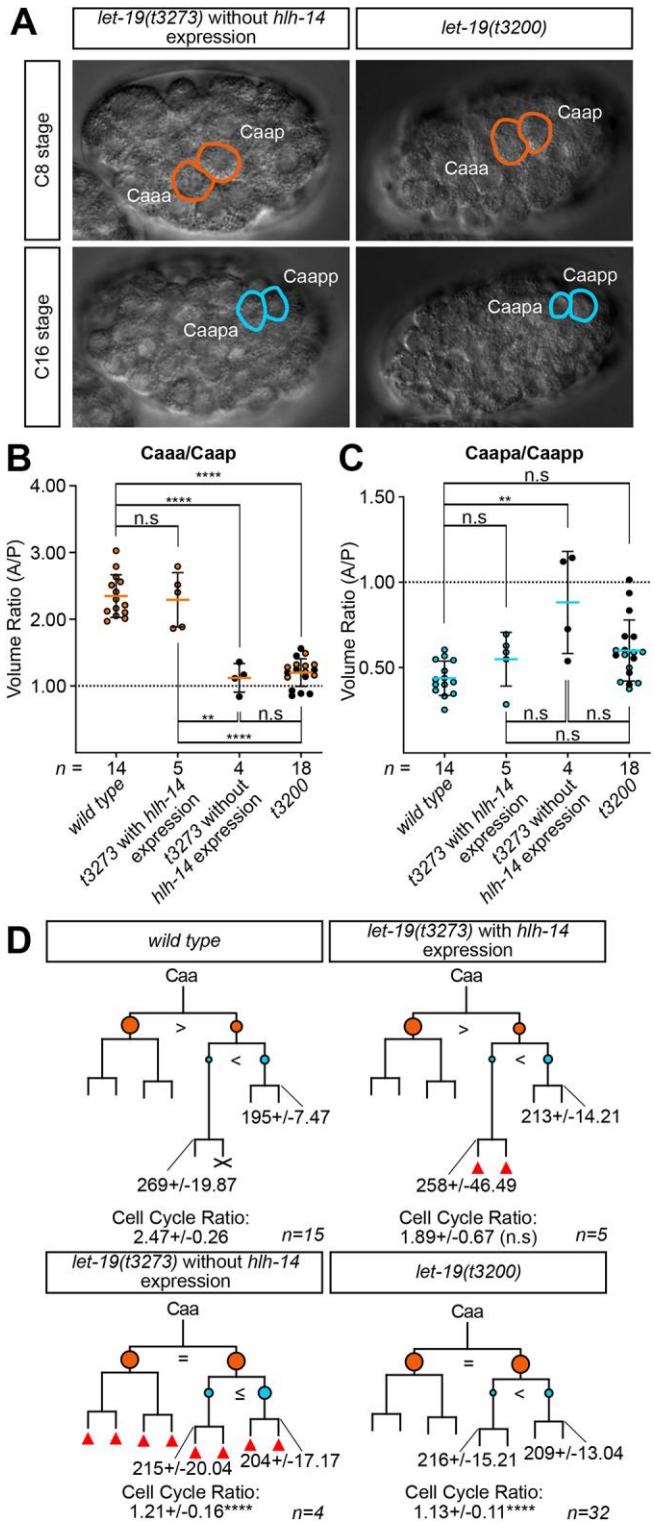


**Fig. 7. *let-19* regulates the unequal cleavage of the Caa and possibly Caap blastomeres**

(A) Representative DIC images of *let-19(t3200)* and *let-19(t3273)* mutants lacking *hlh-14* expression, representing relative daughter cell sizes at the Caa and Caap cleavages. (B) Dot plot of the volumetric ratio of the Caa cleavage in *wild type* and *let-19* mutants, expressed as the anterior/posterior daughter volume, with means and S.D. For *let-*

*19(t3273)* the proportion of embryos that express *hlh-14* are plotted separately from those that do not. *let-19(t3200)* embryos lacking *hlh-14 [gmIs20]* expression are depicted as black. Dotted line indicates an absolute equal cleavage ratio of 1:1. ANOVA: n.s = not significant, ** = p<0.01, **** = p<0.0001. (C) The same as for B but for the Caap cleavage. *let-19(t3200)* embryos lacking *hlh-14 [gmIs20]* expression are depicted in black. ANOVA: ** p<0.01. (D) Lineage diagrams of the neurogenic branch of the C lineage in *let-19* mutants. Branch lengths indicative of division timings. Circles represent relative cell sizes; = represents an equal cleavage, > or < indicate the larger cell. Orange indicates Caa daughters, blue Caap daughters. Red triangle = extra divisions. Caapa and Caapp division times represented in minutes ± S.D., with Cell Cycle Ratio of Caapa/Caapp expression ± S.D. Comparison to *wild type,* ANOVA: n.s = not significant, **** = p<0.0001. For details on *wild type* and mutant genotypes, refer to the materials and methods section.

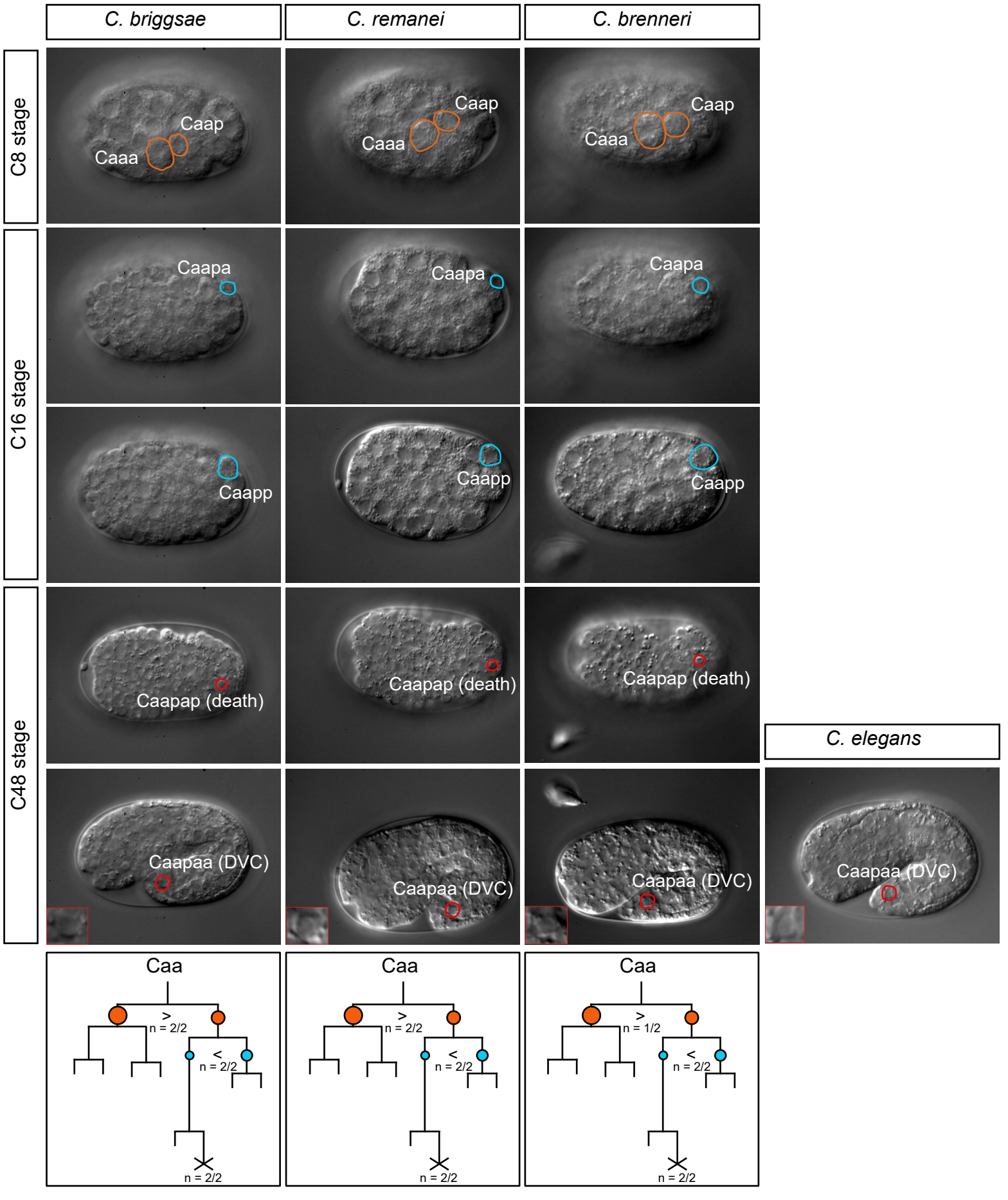

**Fig. S1. Unequal cleavages in the C lineage in other *Caenorhabditis* species** DIC images of the Caa and Caa cleavages, and the Caapap cell death in *C. briggsae, C. remanei* and *C. brenneri*. The Caa cleavage daughters are indicated in orange, the Caap daughter in blue, and Caapa daughters in red. Two images presented when the cells are on different imaging planes. For Caapaa (DVC) an enlarged image is included inset. Cell lineage diagrams of the neurogenic branch based on manually 4D-lineaged embryos, branch length represents division timing. Circles indicate relative size of cells; < or > representing the bias in the unequal cleavage. X represents a cell death. n numbers indicate the number of lineaged embryos displaying the indicated unequal cleavage.

# Figure S2

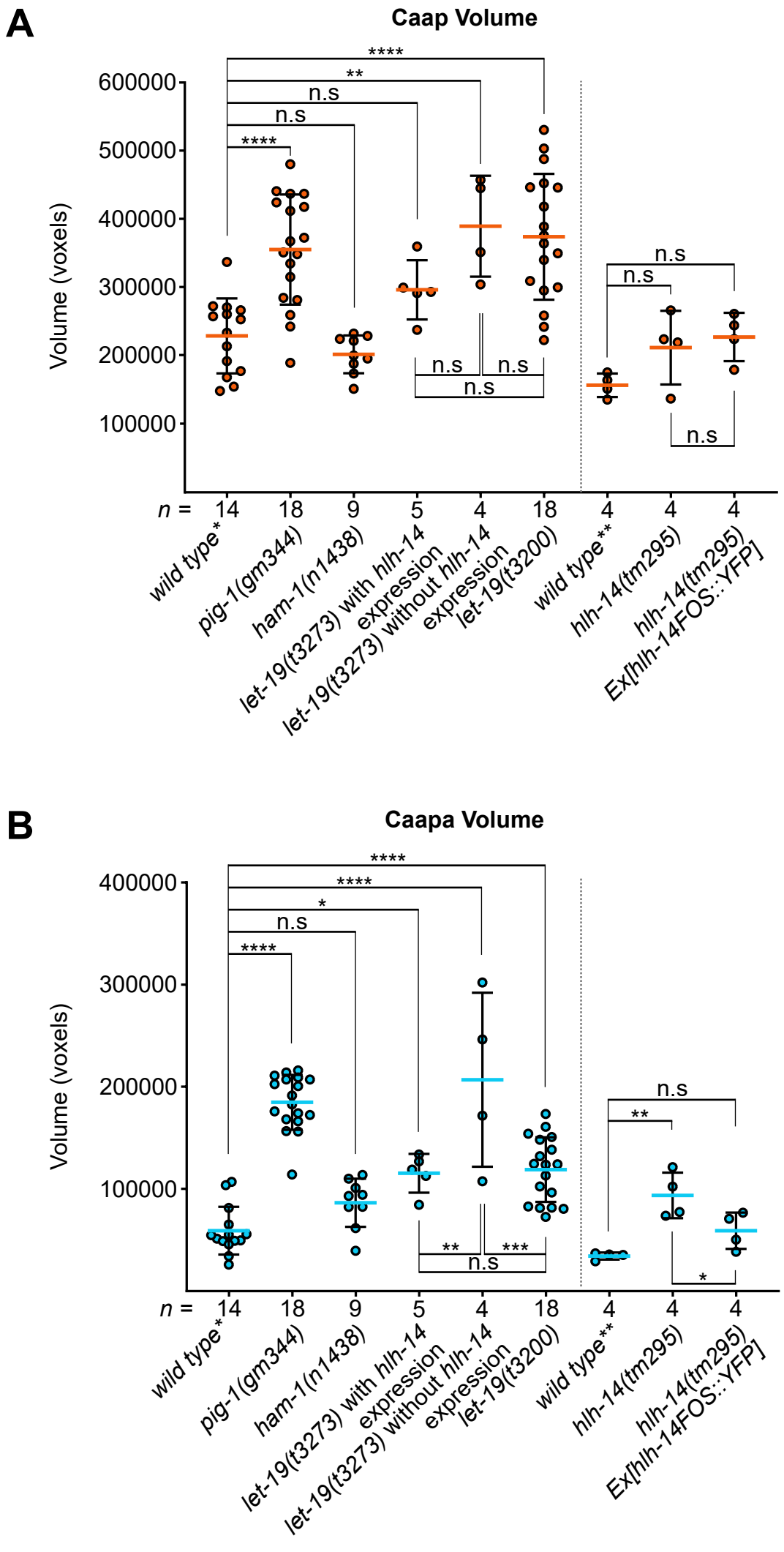

**Fig. S2. Caap and Caapa absolute volumes**

Dot plots of (A) Caap and (B) Caapa absolute volumes (the smaller daughters in *wild type* cleavages) in all strains measured in the study, in voxels, with means and S.D. For *let- 19(t3273)* the proportion of embryos that express *hlh-14* are plotted separately from those that do not. Grey dotted line indicates the separate groups of genotypes compared (those with and without transgenes) and their appropriate *wild type* genotypes. Caap in orange, Caapa in blue as in all other figures. For clarity only comparisons to *wild type* controls and within each mutant group are illustrated (all comparisons computed). ANOVA: n.s not significant, * p<0.05, ** p<0.01, *** p<0.001, **** p<0.0001. *wild type** = *hlh-14 [gmIs20]II* and *hlh-14 [gmIs20] II; dpy-7 [stIs10166]; ceh-63 [otIs458]III*, *wild type*** = N2. For further details on *wild type* and mutant genotypes, refer to the materials and methods section.

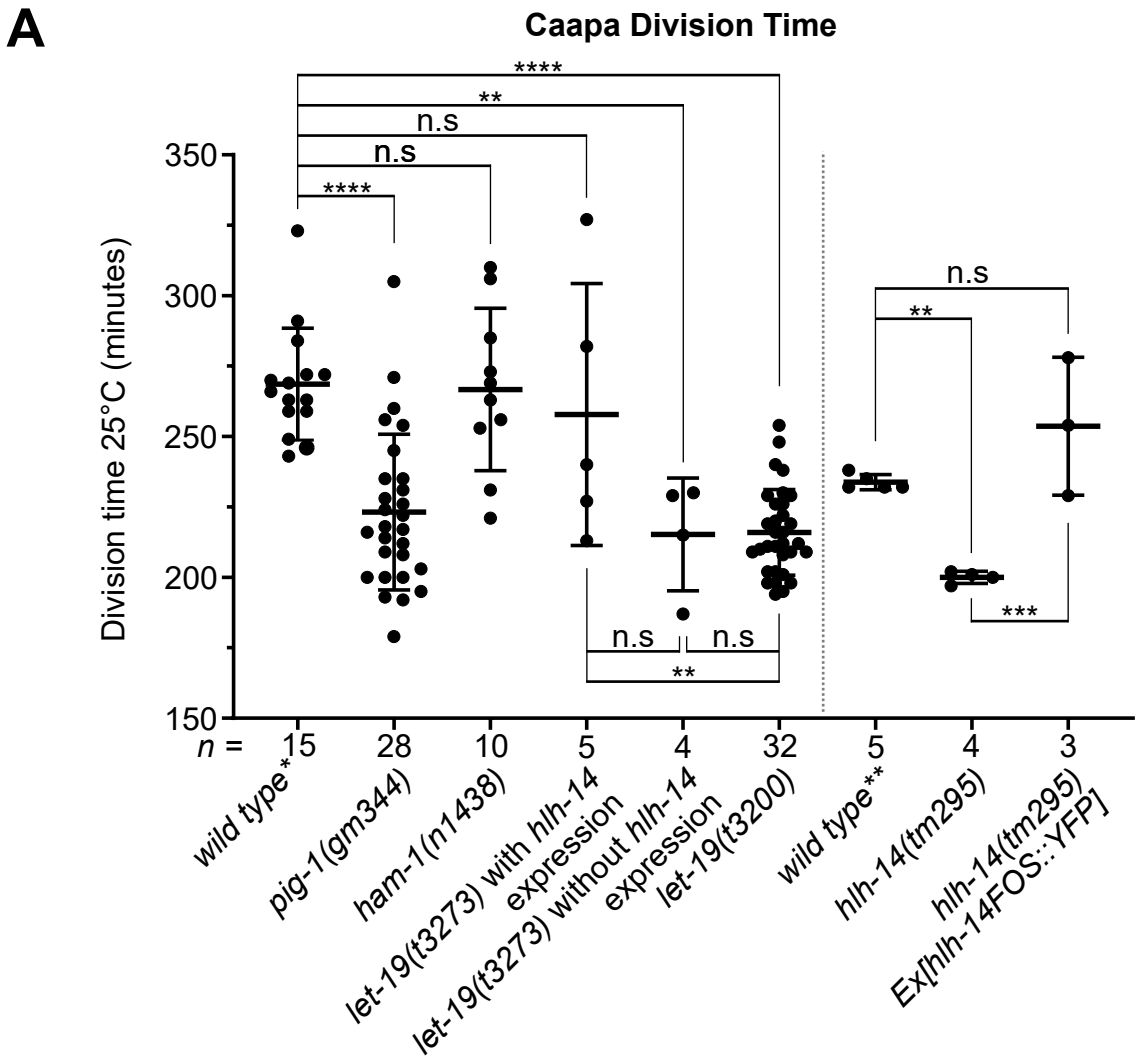


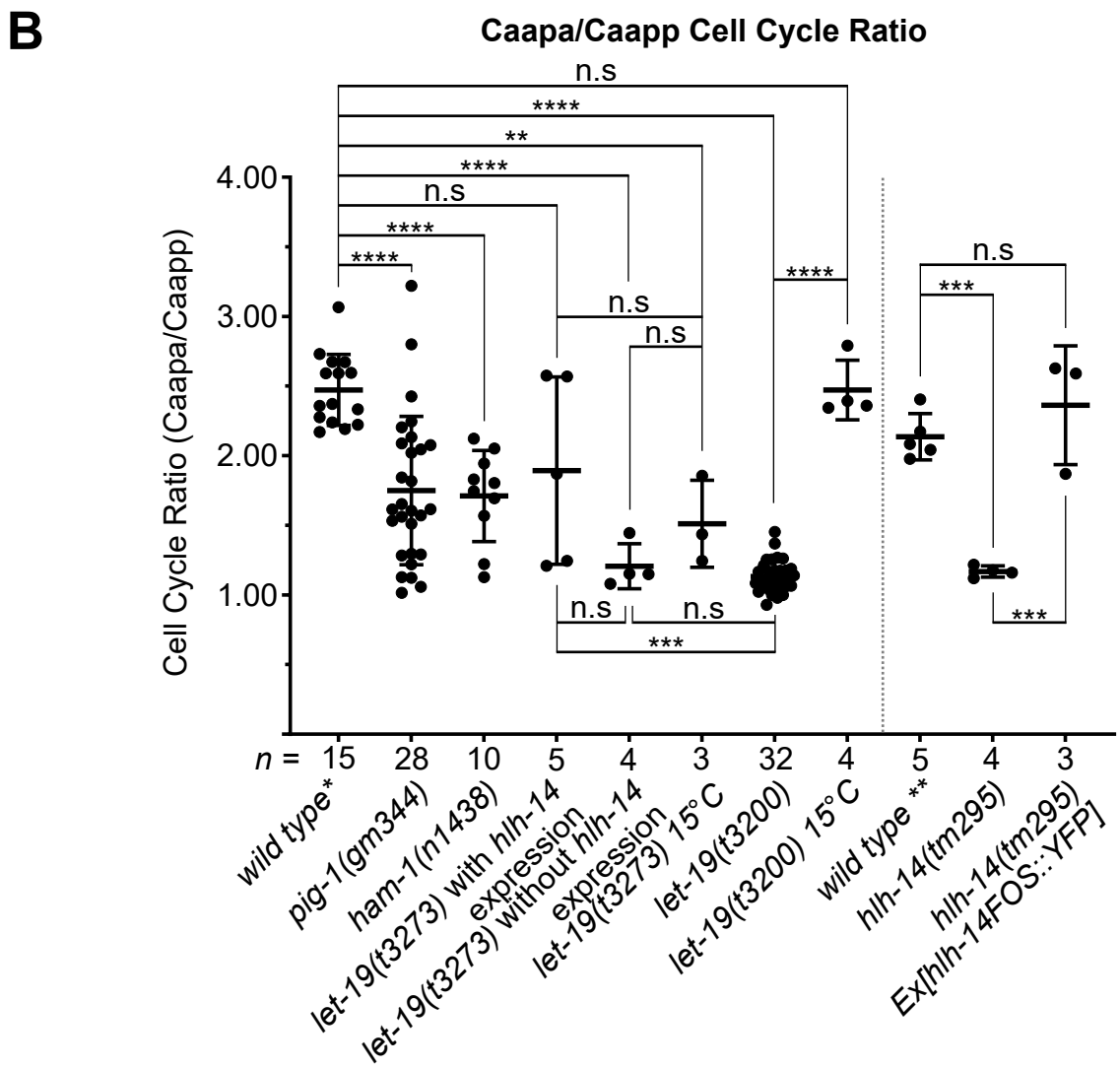

**Fig. S3. Caapa division times and Caapa/Caapp cell cycle ratios**

Dot plots of (A) Caapa division time in minutes at 25°C and (B) Caapa/Caapp cell cycle duration ratio (CCR) in all strains measured for cell volume in the study, with means and S.D. For *let-19(t3273)* the proportion of embryos that express *hlh-14* are plotted separately from those that do not. Grey dotted line indicates the separate groups of genotypes compared (those with and without transgenes) and their appropriate *wild type* genotypes. Caap in orange, Caapa in blue as in all other figures. For clarity only comparisons to *wild type* controls and within each mutant group are illustrated (all comparisons computed). ANOVA: n.s not significant, ** p<0.01, *** p<0.001, **** p<0.0001. *wild type** = *hlh-14 [gmIs20]II* and *hlh-14 [gmIs20] II; dpy-7 [stIs10166]; ceh-63 [otIs458]III*, *wild type*** = N2. For further details on *wild* type and mutant genotypes, refer to the materials and methods section

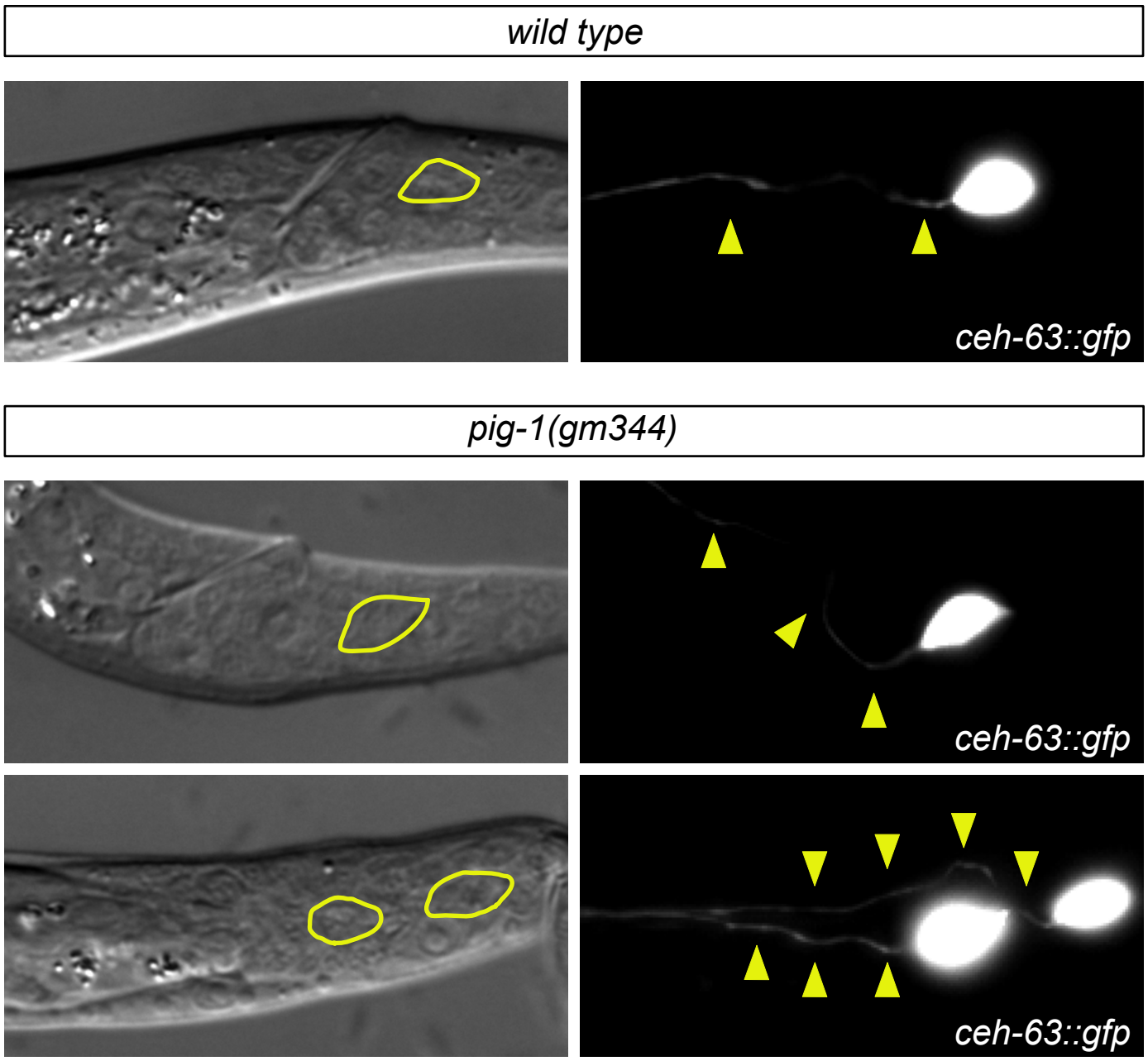


**Fig. S4. DVC neuron morphology in *pig-1(gm344)* L1 larvae**

DIC and GFP images of *ceh-63 [otIs458]* expression in DVC neurons, and so neuronal morphology in hatched *wild type* and *pig-1(gm344)* larvae at the L1 stage. Yellow lines = outline of cell in DIC, yellow arrows = neuronal processes.

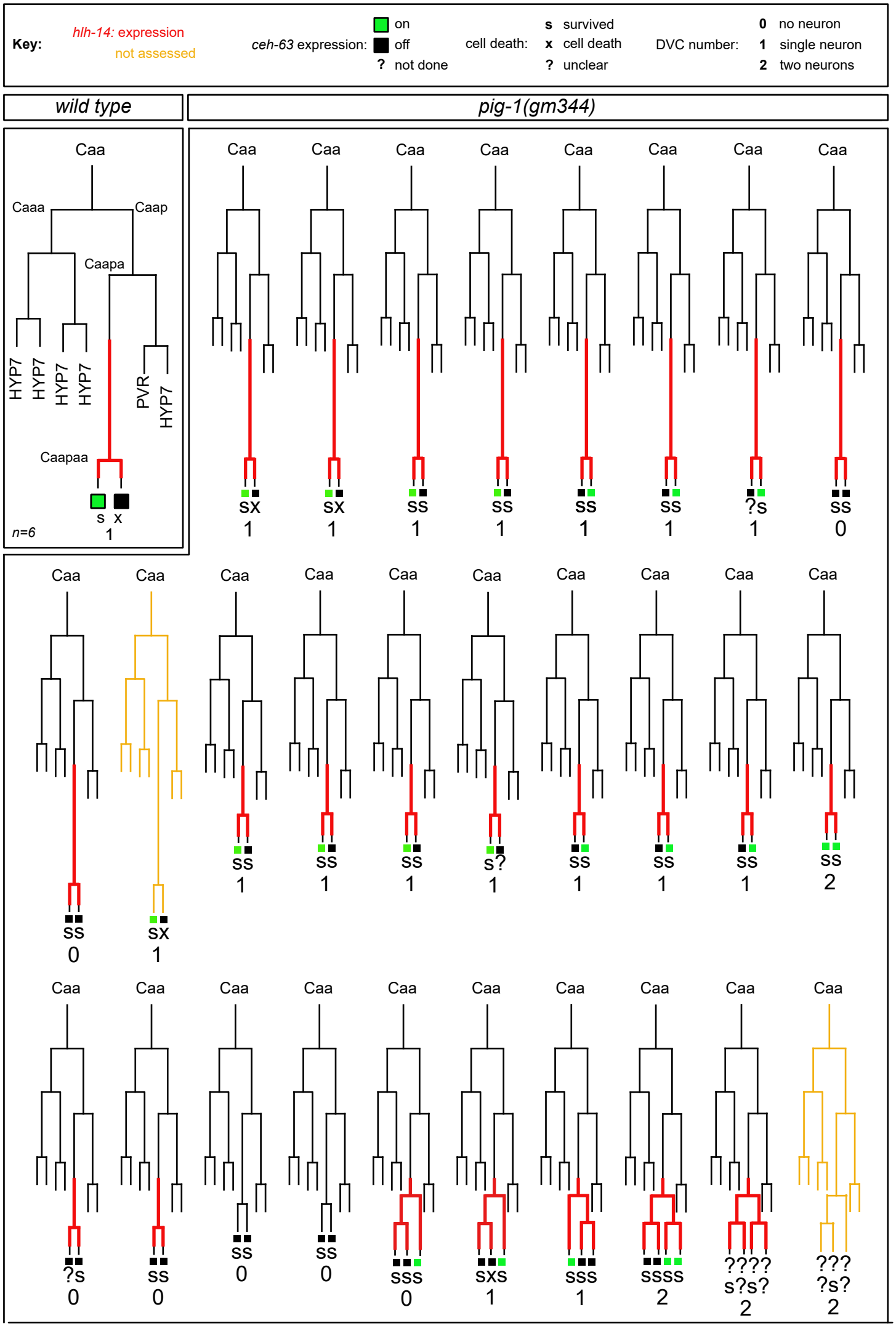

**Fig. S5. Individual lineages of *pig-1(gm344)* mutants**

Lineage diagrams of the neurogenic branch of the C lineage in *wild type* and individual lineaged *pig-1(gm344)* embryos. Branch lengths indicate division times such that precocious divisions are indicated. Red lines represent *hlh-14::gfp [gmIs20]* expression, orange represents embryos in which *hlh-14* expression was not assessed. Terminal phenotypes are represent below each lineage: squares represent DVC neuroblast daughters; green = the expression of *ceh-63 [otIs458]* and DVC fate, black = no expression, ? = unscored. X = cell death , s = survived, ? = unclear/cell lost during lineaging. Number = DVC number as indicated by *ceh-63 [otIs458]* expression.

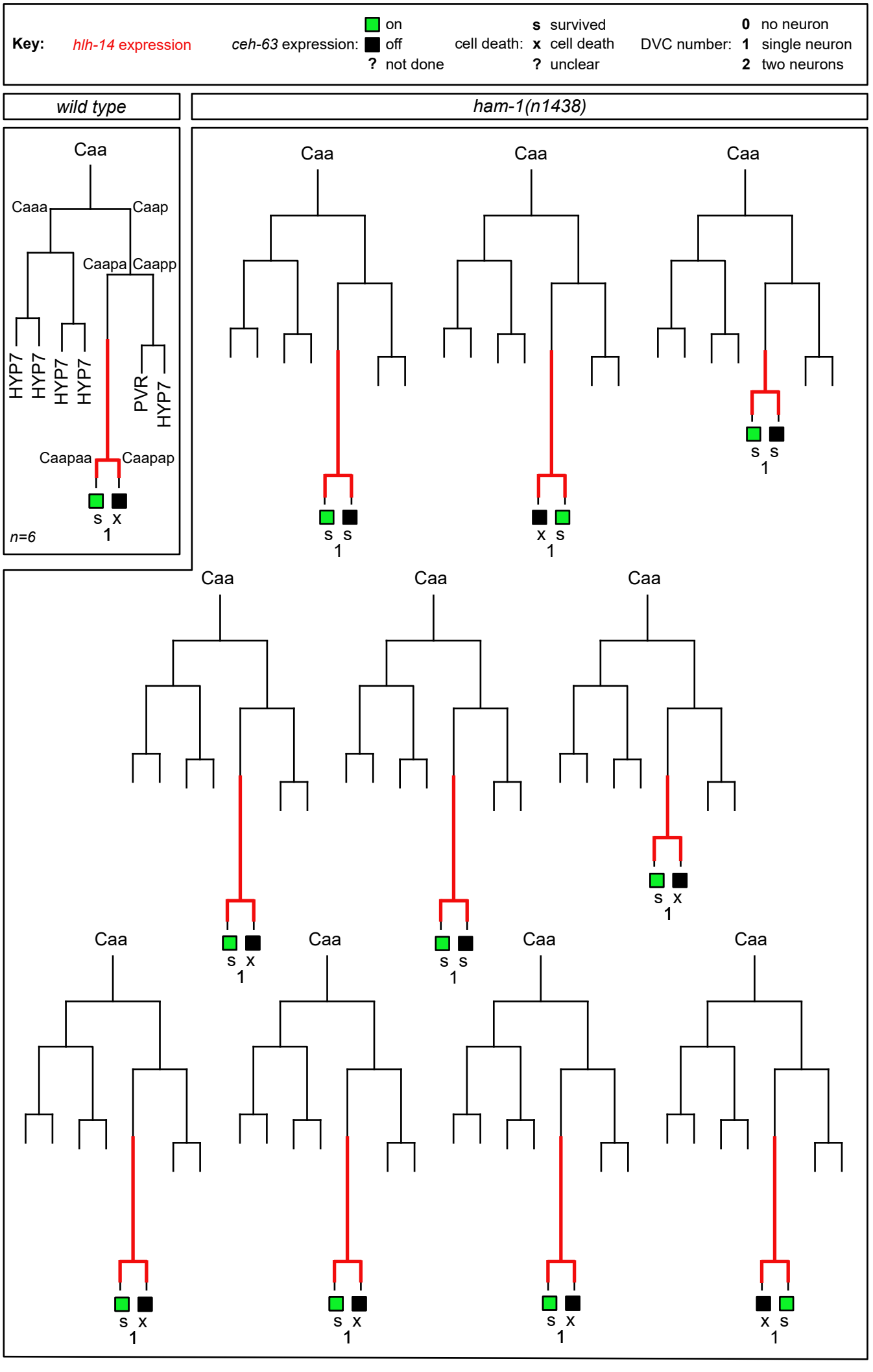

**Fig. S6. Individual lineages of *ham-1(n1438)* mutants**

Lineage diagrams of the neurogenic branch of the C lineage in *wild type* and individual *ham-1(n1438)* embryos. Branch lengths indicate division times such that precocious divisions are indicated. Red lines represent *hlh-14::gfp [gmIs20]* expression, orange represents embryos in which *hlh-14* expression was not assessed. Terminal phenotypes are represent below each lineage: squares represent DVC neuroblast daughters; green = the expression of *ceh-63 [otIs458]* and DVC fate, black = no expression, ? = unscored. X = cell death , s = survived, ? = unclear/cell lost during lineaging. Number = DVC number as indicated by *ceh-63 [otIs458]* expression.

**A** Caapaa and Caapap Nuclei Area in *pig-1(gm344)*

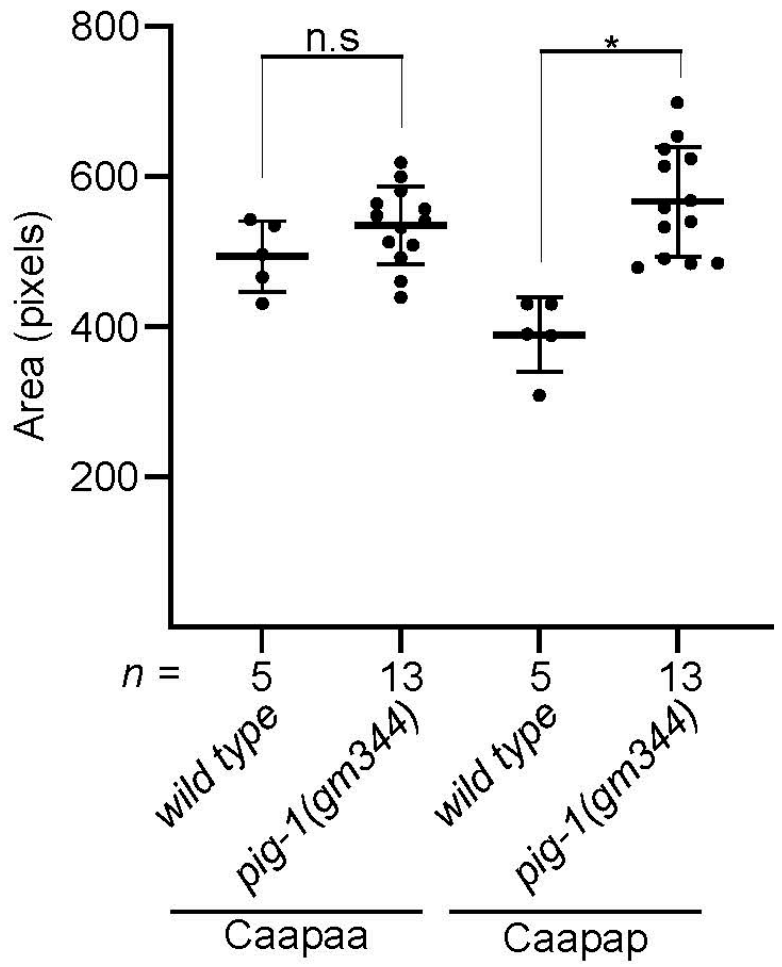


**B** Caapaa Nuclei Area in *pig-1(gm344)* by phenotype

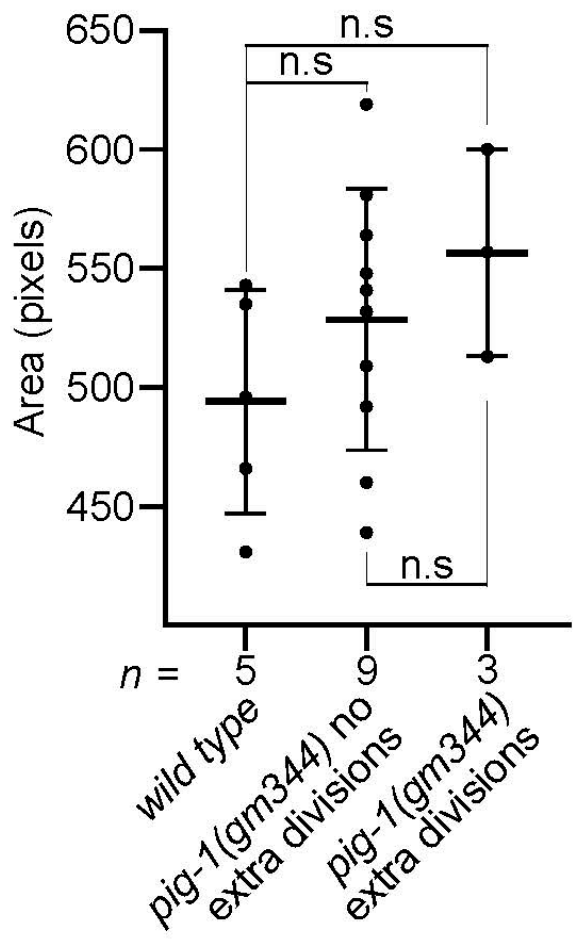

**Fig. S7. Caapaa and Caapap nuclei areas in *pig-1(gm344)* mutants**

(A) Dot plots of Caapaa and Caapap nuclei areas in pixels in *wild type [gmIs20]* and *pig- 1(gm344)* embryos. t-test: n.s = not significant, * = p<0.05. (B) Dot plot of Caapaa nuclei areas in *wild type* embryos and *pig-1(gm344)* embryos plotted separately for whether Caapaa divided again or did not. ANOVA: n.s = not significant. For details on *wild type* and mutant genotypes, refer to the materials and methods section.

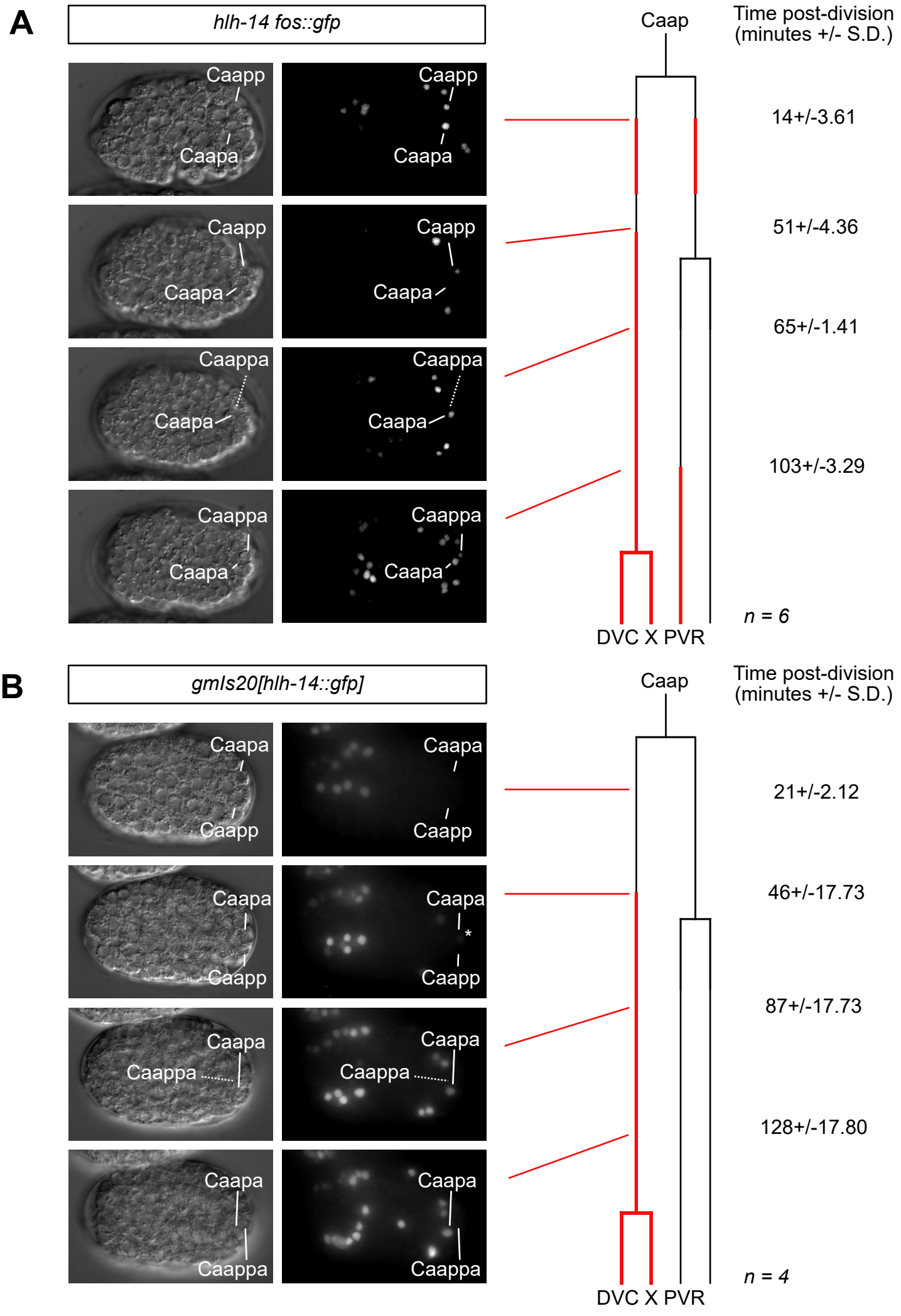

**Fig. S8. Expression of *hlh-14* transgenes following Caap division**

DIC and GFP maximum intensity images from single embryos of *hlh-14* expression, together with lineage diagram for (A) *hlh-14 [gmIs20]* and (B) *hlh-14 fosmid::gfp* transgenes. Cell names are indicated with labels and lines, dotted lines indicate cell position on another plane in DIC. On lineage diagrams branch lengths are indicative to cell cycle duration, red indicated *hlh-14* expression, beginning at the earliest detected time point. Expression patterns are constructed from a consensus of all lineage embryos at 25°C. The fading of *hlh-14 fosmid::gfp* expression at the second timepoint is evident with expression in Caapp fading and Caapa not detected. Timings for the four timepoints shown are indicated as minutes post-division of Caap ± standard deviation.

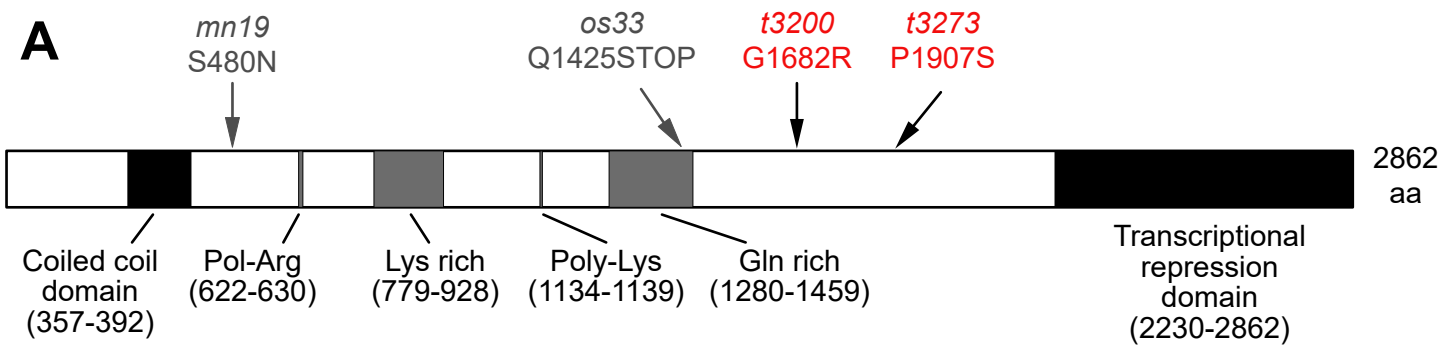


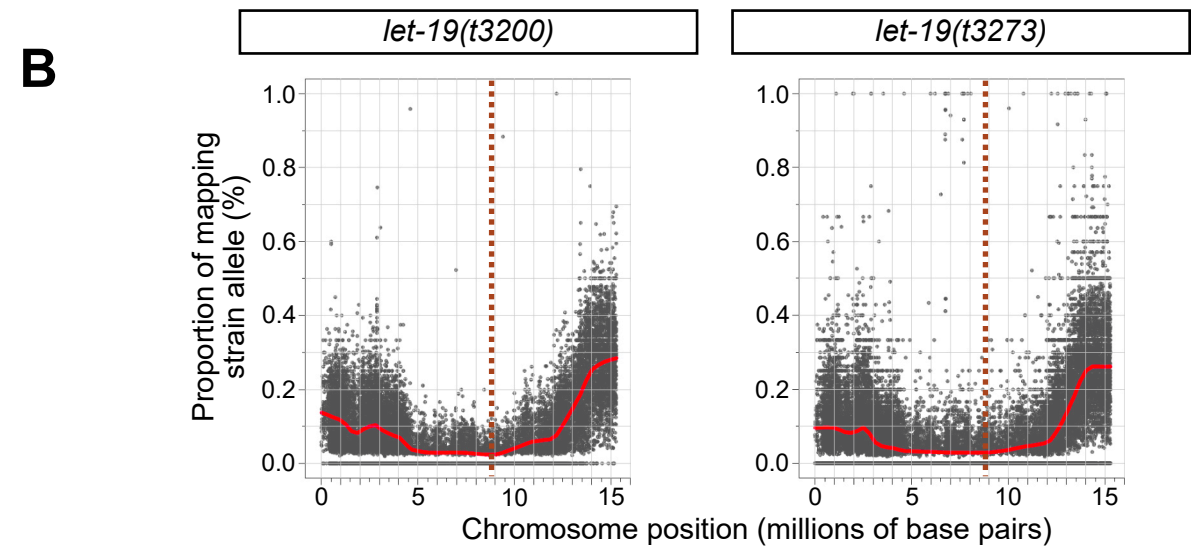


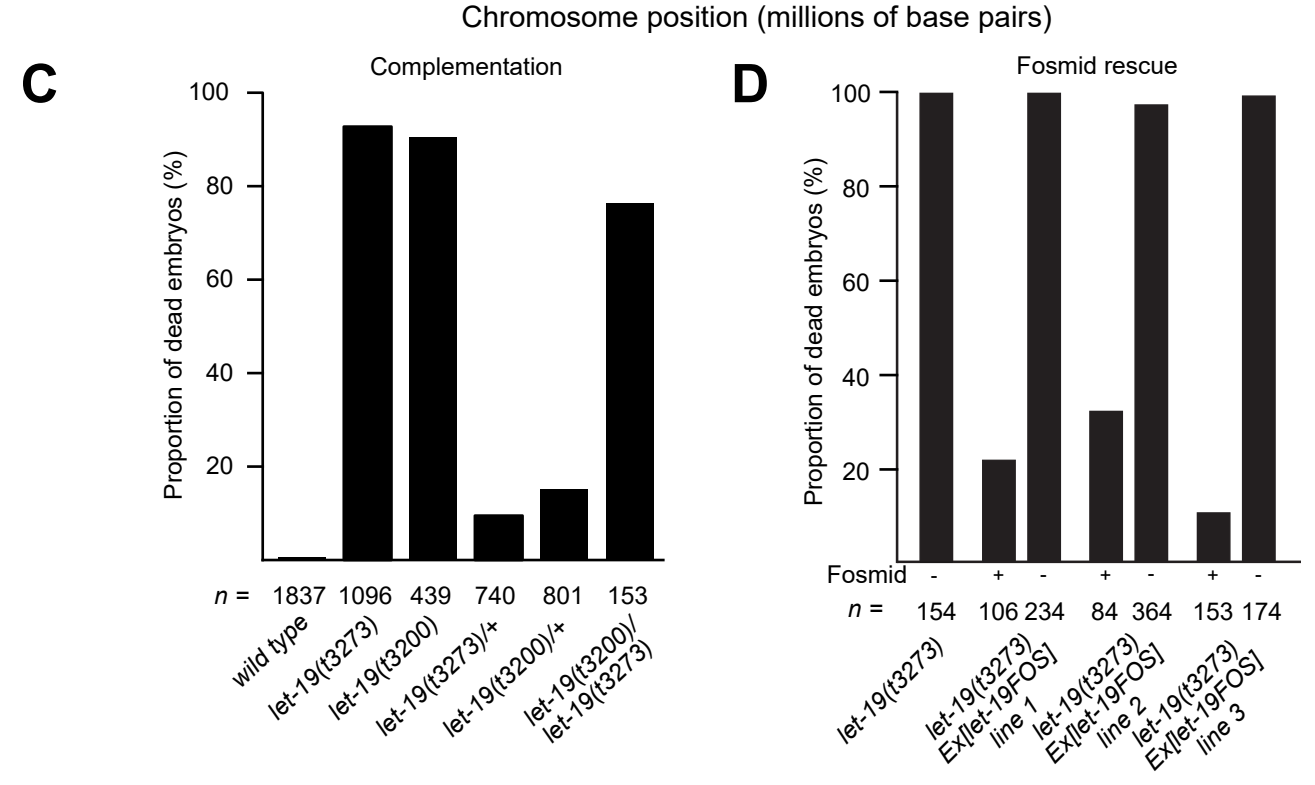


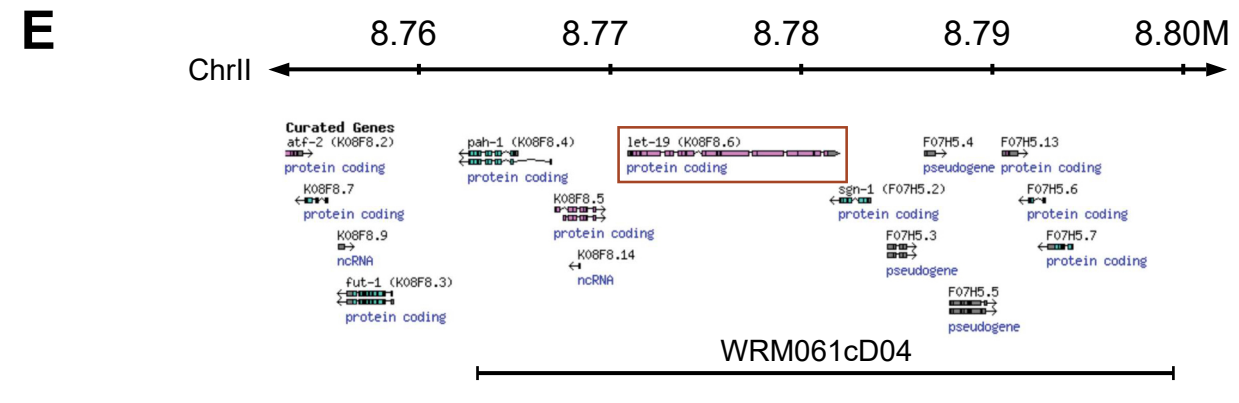

**Fig. S9. Mapping, complementation and rescue of *t3200* and *t3273* as alleles of *let-19***

(A) Diagram of the *let-19* protein structure. Black shading indicates identified domains; grey shading indicates an area rich in the indicated amino acid. The alleles identified in this study and their resultant amino acid changes are indicated in red; other known alleles are indicated in grey. (B) Mapping graphs for *t3200* and *t3273*. The Y-axis is the proportion of the sample containing SNPs from the mapping strain (Hawaiian), a measure of heterozygosity. A value of 1.0 would be entirely Hawaiian, 0.0 entirely from the mutant strain. A red dotted line indicates the location of the causal lesion in the *let-19* locus. (C) A bar chart of the quantification of F1 embryonic or larval lethality at the non-permissive temperature of 25°C from complementation tests between the *t3200* and *t3273* alleles. The graph includes quantification of lethality in maternal effect tests from *wild types* crossed into the mutants. (D) A bar chart of the quantification of F1 embryonic lethality following fosmid rescue. Embryonic lethality scored in three lines containing the WRM061cD04 fosmid covering the *let-19* locus; + indicates the presence of the fosmid, - indicates its absence. For both *t3200* and *t3273* strains, *let-19* was the only gene containing a lesion covered by WRM061cD04. (E) Diagram of the region on chromosome II containing the *let-19* locus, adapted from the genome browser accessed via wormbase.org. The *let-19* locus is indicated by a red box. The region covered by the WRM061cD04 fosmid is indicated below the depiction of the genes in the region.

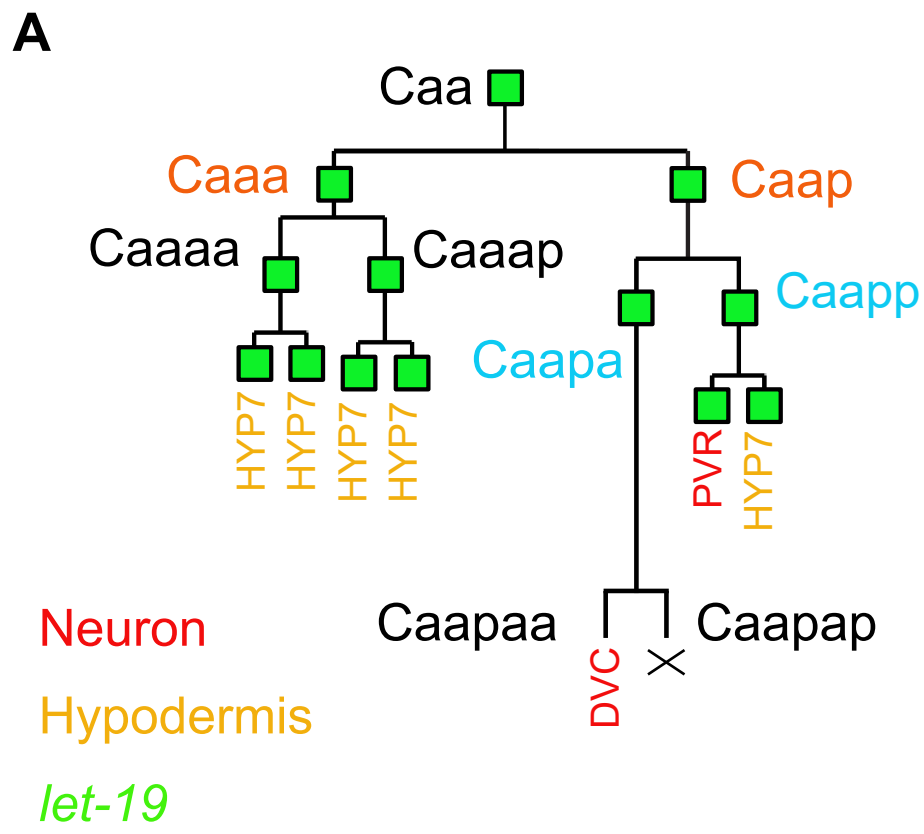


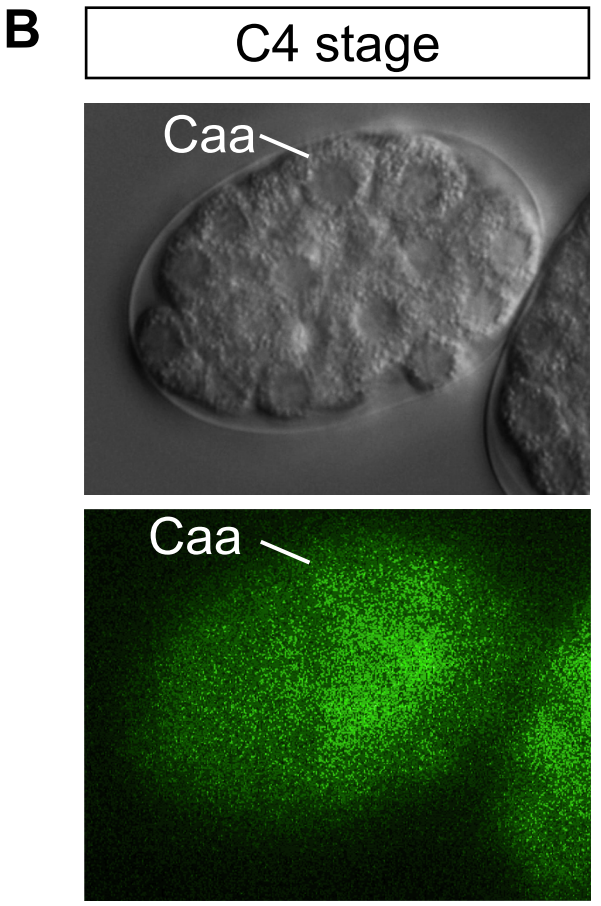


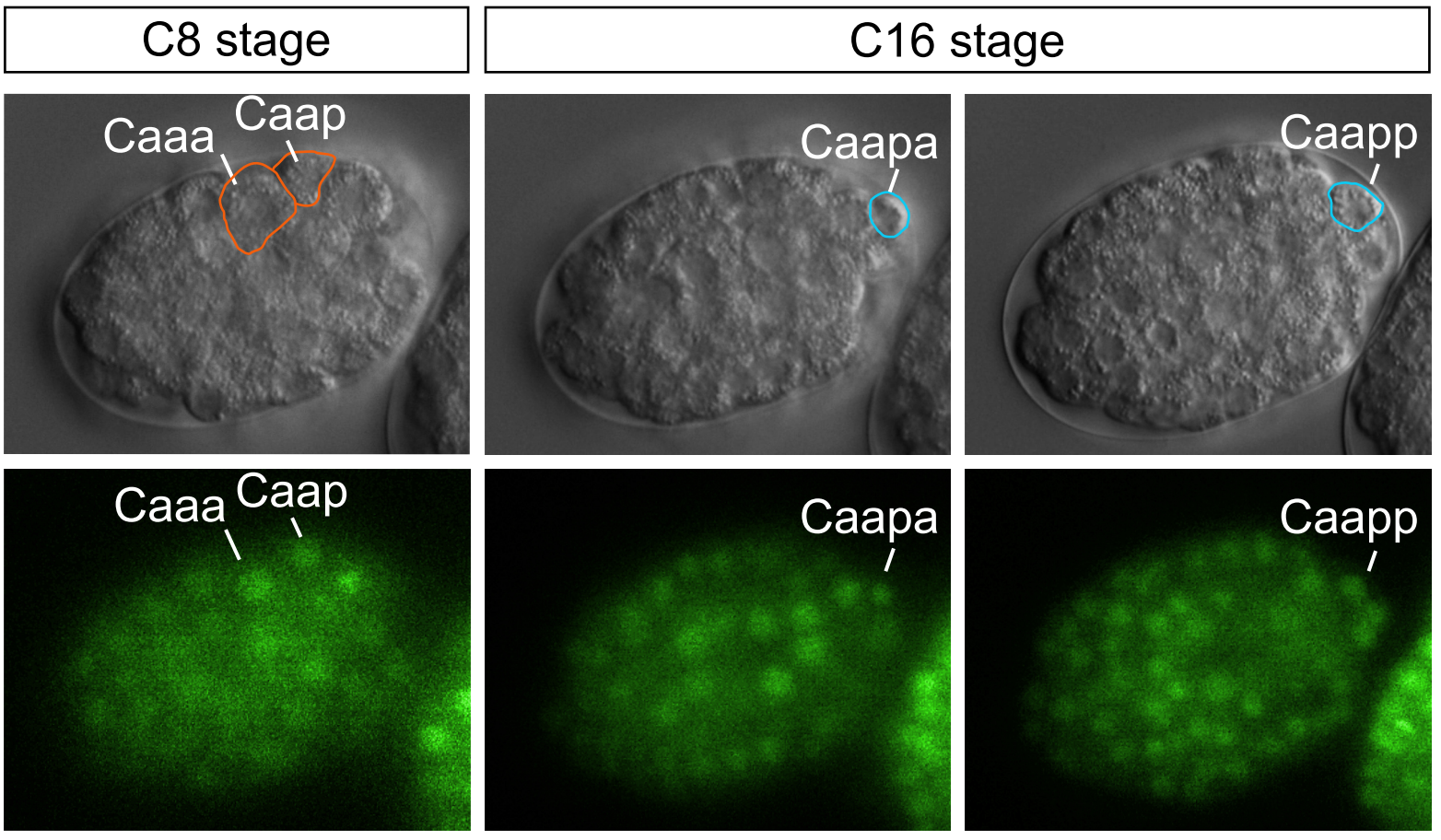

**Fig. S10. Expression of *let-19* in the C lineage cleavages**

(A) Lineage diagram of the C lineage branch descended from Caa. Squares indicate cells scored for expression of *let-19*, solid green indicating expression. Red text indicates neurons, yellow indicates hypodermis. The cell names of Caa daughters are in orange, Caap daughters in blue, as in other figures. (B) DIC and GFP images of *let-19* expression in the mother and daughter cells of the unequal cleavages studied (Caa, Caaa. Caap. Caapa, Caapp). Caa daughters are indicated in orange, Caap daughters in blue, as in all other figures.

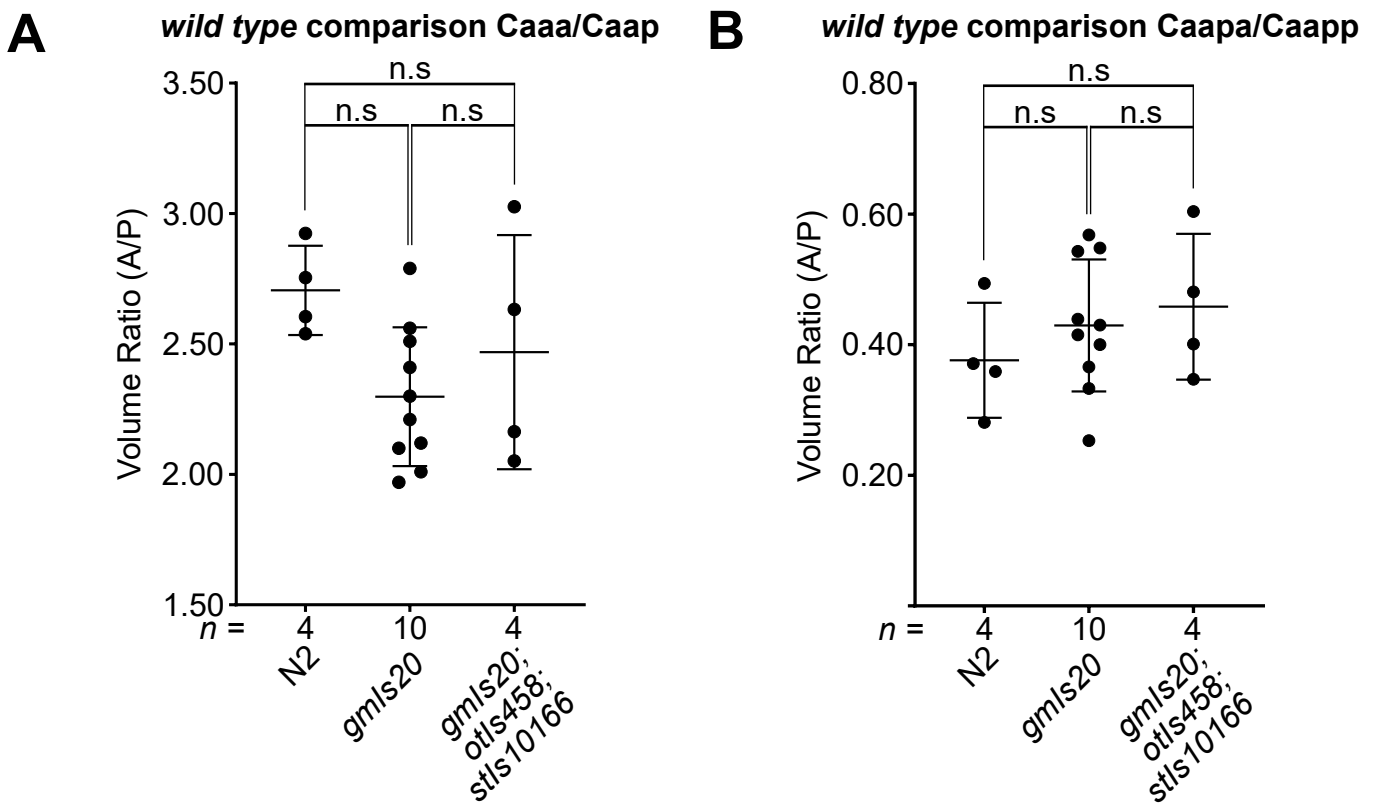


**Fig. S11. Comparison of Caa and Caap division ratios and Caap and Caapa absolute volumes in *wild type* genotypes**

Dot plots of the volumetric ratio of the (A) Caa and (B) Caap cleavages in N2, *hlh-14 [gmIs20]* carrying and *hlh-14 [gmIs20], dpy-7 [stIs10166], ceh-63 [otIs458]* transgene carrying embryos expressed as the anterior daughter volume/posterior daughter volume, with means and S.D. ANOVA: n.s = not significant. Dot plots of absolute volume of (C) Caap and (D) Caapa in voxels in N2, *hlh-14 [gmIs20]* carrying and *hlh-14 [gmIs20], dpy-7 [stIs10166], ceh-63 [otIs458]* transgene carrying embryos. ANOVA: n.s = not significant, ** = p<0.01.